EVOLUTION OF FINE-GRAINED CHANNEL MARGIN DEPOSITS BEHIND LARGE WOODY DEBRIS IN AN EXPERIMENTAL GRAVEL-BED FLUME

by

Bridget O'Neill

A thesis submitted to the Faculty of the University of Delaware in partial fulfillment of the requirements for the degree of Master of Science in Geology

Summer 2015

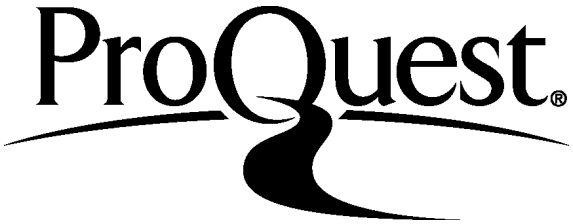

EVOLUTION OF FINE-GRAINED CHANNEL MARGIN DEPOSITS BEHIND LARGE WOODY DEBRIS IN AN EXPERIMENTAL GRAVEL-BED FLUME

by

Bridget O'Neill

Approved: _____
James Pizzuto, Ph.D.
Professor in charge of thesis on behalf of the Advisory Committee

Approved: _____
Neil Sturchio, Ph.D.
Chair of the Department of Geological Sciences

Approved: _____
Dr. Mohsen Badiey, Ph.D.
Interim Dean of the College of Earth, Ocean, and Environment

Approved: _____
James G. Richards, Ph.D.
Vice Provost for Graduate and Professional Education

ACKNOWLEDGMENTS

Thank you to my advisor, Dr. Jim Pizzuto for his guidance, support, and encouragement throughout this project. I also appreciate the assistance and input provided by my committee members, Dr. Jack Puleo and Dr. Katherine Skalak. A major thank you goes to Peter Wilcock and Ciaran Harman who allowed me to utilize the flume at John Hopkins University.

I would also like to thank Sam Mark, a talented REU student, who was a major part of my team, assisting in the operation of the experiments. I would also like to acknowledge Caraline Canning and Jeremy Keeler who were flume assistants. I would like to thank my research group: Tobias Ackerman, Adam Pearson, Michael Orefice, Dale Lambert, and Margaret Christie for their feedback and assistance throughout this project. Much gratitude is also given to Bill Parnella and Craig Prettyman.

Additionally, much thanks goes to those who provided endless support and encouragement. My roommates, Alex and Tom, provided much needed laughter and food throughout this process. Friends such as Steve Wagner, Keri Fischer, and Erika Schrieber, were great listeners who would hear my struggles and give advice. Lastly parents, Mary-Grace and Kevin, my sister Molly, and my brother Daniel gave me love, support and encouragement.

Financial support for this project was partially supported by NSF Award EAR1331856, "Christina River Basin CZO: a whole watershed approach to integrating feedbacks between water, mineral and carbon fluxes in human landscapes."

TABLE OF CONTENTS

LIST OF TABLES

LIST OF FIGURES

ABSTRACT

Fine-grained channel margin (FGCM) deposits of the South River, Virginia sequester a substantial volume of fine-grained sediment behind large woody debris (LWD). FGCM deposits were created in a laboratory setting meant to simulate the South River environment using a recirculating flume (15 m long by 0.6 m wide) with a fixed gravel bed and adjustable slope (set to 0.0067) to determine how fine sediment is transported and deposited behind LWD. Two model LWD structures were placed 3.7 m apart on opposite sides of the flume. A wire mesh screen with attached wooden dowels simulated LWD with an upstream facing rootwad. Six experiments with three different discharge rates (0.017 m^3/s, 0.025 m^3/s, and 0.031 m^3/s), each with low and high sediment concentrations, were run. Suspended sediment was very fine-grained (median grain size of 0.10 mm) and very well sorted (0.03 mm) sand. Upstream of the wood, water depths averaged about 0.083 m, velocities ranged from 0.33 m/s to 0.40 m/s, and Froude numbers averaged around 0.41. Downstream of the first LWD structure, velocities were reduced tenfold. Small amounts of sediment passed through the rootwad and fell out of suspension in the area of reduced flow behind LWD, but most of the sediment was carried around the LWD by the main flow and then behind the LWD by a recirculating eddy current. Upstream migrating dunes formed behind LWD due to recirculating flow. These upstream migrating dunes began at the reattachment point and merged with deposits formed from sediment transported through the rootwad. Downstream migrating dunes formed along the channel margin behind the LWD, downstream of the reattachment point. FGCM deposits were about 3 m long, with average widths of about 0.8 m. Greater sediment concentration created

thicker FGCM deposits, and higher flows eroded the sides of the deposits, reducing their widths.

Chapter 1

INTRODUCTION

Sediment erosion and deposition shape the landscape and move nutrients and pollutants. Sediment is transported by fluid (water, wind, ice) or by sediment-gravity-flows (debris flows, mudslides) (Ritter, Kochel, & Miller, 2011). Fluid flows, especially fluvial transport of sediment, contribute to geomorphic evolution of landscapes. Understanding the fluvial processes that control sediment transport contributes to quantifying the movement of nutrients and contaminants that adhere to sediment.

Fine-grain channel margin deposits (FGCM), a type of geomorphic feature (Skalak & Pizzuto, 2010), are depositional features within gravel-bed river channels that store fine sediment. The features typically occur on channel margins near large woody accumulations. The hydraulic and sediment processes that contribute to the formation of these deposits are poorly understood. This study seeks to explain the fluvial processes of sediment transport and deposition that result in the formation of FGCM deposits.

1.1 Sediment Transport

Movement of material by fluvial processes is typically categorized by the mode of transport downstream. Three main categories, bed load, suspended load, and dissolved load describe sediment transport within rivers. The bed load is material that is transported close to or along the bottom of the channel by rolling, bouncing, or

sliding. Suspended material is transported in suspension, rarely being deposited. The dissolved load is material that is carried in solution.

1.2 Suspended Sediment

Suspended sediment is maintained in suspension due to lifting forces due to turbulence of the stream flow. The turbulence levels must be equal to or greater than the particle fall velocity to create suspended material (Mangelsdorf, Scheurmann, & Weib, 1990). Particle deposition occurs when turbulence levels decrease allowing the particle to settle out of suspension.

Suspended sediment is often the largest component of fluvial sediment transport (Knighton, 1998). In the South River of Virginia, where FGCM deposits were first identified (Skalak & Pizzuto, 2010), the annual suspended sediment load is approximately 5200 metric tons (Pizzuto , et al., 2006). Other estimates by Eggleston (2009) and Lawler, Matusky, and Skelley Engineers (1981) estimate the annual suspended sediment transport at Waynesboro to be 9050 and 3500 metric tons, respectively.

Fine sediments, typically transported as suspended sediment, influence ecological processes and cycling of contaminants and nutrients. Fine sediments include sand, silt, clay, and fine organic matter. Nutrients, heavy metals, and hydrophobic pollutants adhere to fine particles typically transported as suspended sediment (Foster & Charlesworth, 1996; Miller, 1997). Suspended sediment also influences the habitat of benthic macroinvertebrates (Wood & Armitage, 1997; Petts, 1984) and some fish species (Bruton, 1985; Lisle, 1989; Kondolf, Sale MJ, & Wolman, 1993). Suspended sediment transport within high-order, lowland gravel-bed

rivers has significant geomorphic effects by influencing stream behavior and channel form.

1.2.1 Wash Load Component of Suspended Sediment

Suspended sediment particles that are finer than 0.064 mm and easily moved in suspension are classified as ‘wash load’. The wash load is primarily controlled by the supply rate of water and sediment from the drainage basin rather than the transport capacity of the stream. Moreover, the wash load is generally thought as throughput within the fluvial system, comprising the dominant part of the sediment yield, or total sediment outflow from a watershed. The suspended particles move approximately at the same speed as flow, settling out only where flow velocities are greatly reduced (Knighton, 1998). The wash load concept assumes that the velocity within the channel if often too high for fine sediment deposition limiting storage of fine sediment to the floodplain, hyporheic zone (Owens, Walling, & Leeks, 1999; Phillips & Walling, 1999), channel backwaters (Schmidt, et al., 2001), and point bars (Nanson, 1981). Knowledge of the transport and deposition of fine-grained particles in a river is fundamental to understanding nutrient and pollutant cycling.

1.3 FGCM deposits

FGCM deposits consist of sand, silt, clay, and organic material; sediments that should remain suspended in a gravel-bed river. These deposits accumulate downstream of large woody debris (LWD) along the margins of the wetted perimeter of the channel (Skalak & Pizzuto, 2010). The hydraulic processes that encourage FGCM deposits have not been evaluated nor have the conditions that promote their formation.

1.3.1 The Hydraulic and Geomorphic Setting of the South River

FGCM deposits were first identified in South River, VA. The South River is a single-thread, sinuous, gravel-bed river located in the Valley and Ridge Geomorphic Province of Virginia. South River flows north form Waynesboro to Port Republic, Virginia where it merges with the North River to form South Fork of the Shenandoah River (Skalak K. , 2009). The channel of South River has an average sinuosity of 1.4 (Narinesingh, 2010) and a slope of 0.0013 in upstream sections and 0.0024 farther downstream (Skalak & Pizzuto, 2010). The Manning's roughness value for the channel is 0.03, based on calibrated HEC-RAS modeling by URS Corp (Pizzuto 2012). Channel width is about 20 - 40 m typically and the average bank height is 1.5 m (Rhoades et al., 2009; Pizzuto and O'Neal, 2009; Hess, 2007). FGCM deposits most likely form at discharges less than those which produce bankfull depth. A channel depth of 1 m will be assumed for calculations of South River hydraulic conditions, in addition to calculations using bankfull depth.

Channel banks are comprised of silt and clay, with some sand and gravel (Rhoades et al, 2009; Pizzuto and O'Neal 2009). Bed material is comprised of sand, granules, pebbles, cobbles, and boulders with frequent bedrock exposures along the bed and the banks (Skalak & Pizzuto, 2010). Pomraning (2011) measured the size distribution of the bed material by pebble counting (Wolman, 1954). She found the median sediment diameter to be 25.5 mm and the 84^{th} percentile grain diameter to be 57.8 mm. Approximately 5.7% of the sediment consists of sand (with a diameter smaller than 2 mm).

The U.S. Geological Survey maintains gaging stations along the South River at Waynesboro, Dooms, and Harriston. Discharge values for these locations along South River are given in Table 1.1. Median discharge for the Waynesboro location, is 1.57

m^3/s. Discharge data from October 2007 for the Waynesboro gage is shown in Figure 1.1.

Table 1.1 U.S. Geological Survey discharge data and other select information from gage stations on South River. The Waynesboro data were based on 62 years of data while the Dooms and Harriston sites were based on 32 and 73 years of data, respectively.

Station	Waynesboro	Dooms	Harriston
Drainage Area (km^2)	329	383	549
Median Discharge (m^3/s)	1.57	2.55	3.09
Mean Discharge (m^3/s)	2.01	2.97	3.68
25^{th} Percentile (m^3/s)	1.16	2.03	2.43
75^{th} Percentile (m^3/s)	2.03	3.17	3.76
Minimum (m^3/s)	0.51 (2002)	1.47 (1977)	1.07 (2002)
Maximum (m^3/s)	11.49 (1995)	13.68 (1995)	18.97 (1972)

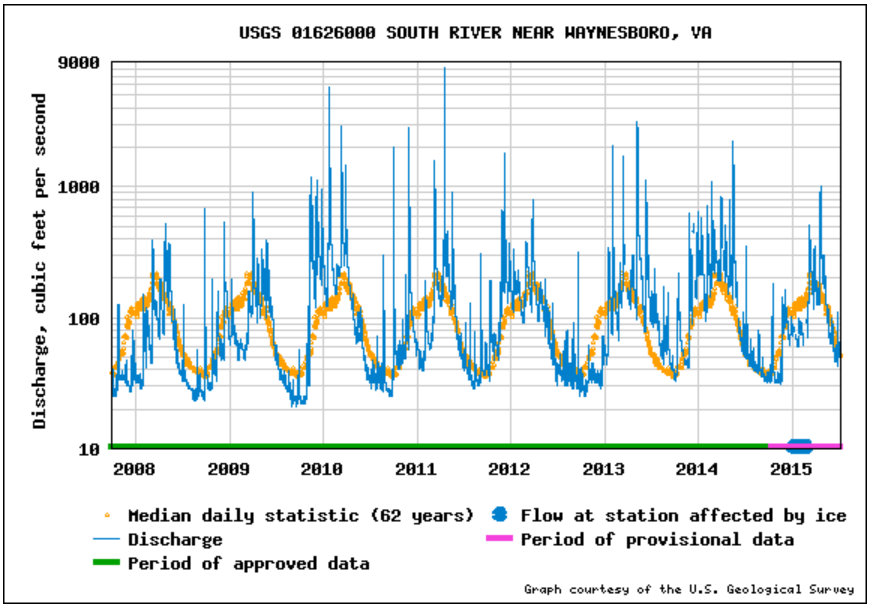

Figure 1.1 Daily discharge data from U.S. Geological Survey for South River near Waynesboro, VA from October 2007 to July 2015.

1.3.2 FGCM characteristics

FGCM deposits represent a significant portion of sediment storage. Within South River, Skalak and Pizzuto (2010) found that FGCM deposits store a total mass equivalent to 17 % to 43 % of the annual suspended sediment load. In their 37 km study reach, 54 deposits were mapped. The deposits account for a total of 2150 m^3 (1505 tons) of stored sediment. The deposits average 42 ± 58 m long, 5 ± 2 m wide, and 0.34 ± 0.18 m thick. The average grain size composition for the deposits is 23% clay, 23% silt, and 54% sand. FGCM deposits do not occur where the slope of the river exceeds 0.0025. The majority of FGCM deposits occur in the upstream end of the study reach where the average channel slope is 0.0013; only a few occur in the downstream study reach where the slope averages 0.0024 (Skalak & Pizzuto, 2010).

1.3.3 Role of LWD in formation of FGCM deposits

FGCM deposits likely form in areas of reduced velocity downstream of accumulations of LWD. Therefore, the accumulation of LWD likely influences the formation of FGCM deposits (Skalak & Pizzuto, 2010). In the South River, LWD typically accumulates as isolated logs and small jams along the margins of the channel. The LWD is smaller than the channel width and thus its distribution is governed by channel morphology (Hess, 2007). In smaller headwater channels, the wood itself typically controls pool and riffle spacing and other aspects of fluvial morphology (Abbe and Montgomery, 1996; Gurnell et al., 2002; Webb and Erskine, 2003).

Once LWD has accumulated, the wood affects hydraulic processes, which in turn affects sediment transport. LWD accumulations generate area of low velocity and shear stress which promote sediment deposition (Fetherston et al., 1995; Daniels,

2003; Daniels and Rhoads, 2003). Sediment has been observed to accumulate downstream of LWD obstructions in low-energy systems; in high-energy systems, sediment storage occurs upstream of the LWD (Gurnell and Gregory, 1995). Removal of LWD structures form stream channels causes rapid release of sediment from these areas of storage (Smith et al., 1993; Ralph et al., 1994; Gurnell and Gregory, 1995).

LWD accumulations likely control the development of FGCM deposits by creating areas of reduced velocity, turbulence, and shear stress in the lee of the wood. Deposition would most likely be punctuated by periods of erosion and non-deposition. The deposit may reach a maximum size once the area of reduced velocity created by the LWD obstruction is filled with sediment. The longevity of the deposit would depend on the presence of the LWD obstruction; the deposit would most likely be eroded if the LWD obstruction is washed away (Skalak & Pizzuto, 2010).

1.4 Objectives of Study

The goal of this study is to extend the analysis of the formation and evolution of FGCM deposits previously accomplished by Skalak (2009) and Skalak and Pizzuto (2010). The purpose of this project is to characterize the deposition and erosion of fine-grained sediments in a gravel-bed river in relation to discharge, LWD, and sediment concentration. The study will physically model stream processes using a flume. The main objectives of flume experiments are:

1. Determine if a threshold exists that defines a limit of discharge for which deposits will or will not occur.
2. Measure and assess the hydraulic conditions (velocity, near bed Reynolds stresses, and turbulent kinetic energy) upstream of, adjacent

to, and downstream of the LWD for cases of deposition, no deposition, and erosion.

3. Monitor the size and geometry of deposits as they evolve.
4. Draw conclusions from the results of the flume experiments that define a likely outcome of comparable conditions in a real world system.

Chapter 2

METHODS

2.1 Introduction

Complex multivariate relationships that vary both spatially and temporally often control fluvial processes and form. Detailed field monitoring of these processes can provide accurate data but generally will not provide understanding of multivariate controls on the system. Numerical modelling allows for better understanding of complex interrelationships between variables but depends on limited data and simplified assumptions. A third technique, physical modelling allows for controlled laboratory analysis, usually on a reduced time scale, of select variables on fluvial processes and morphology.

Physical models allow researchers to monitor the influence of selected factors without variability in the elements of the system. Physical models are simplified versions of a prototype. In addition to holding variables constant, these models allow for the replication of a study to determine relationships between variables and features.

In the South River system, LWD obstructions are one of numerous variables that control sediment transport and deposition. The magnitude and time distribution of discharge within the stream system, along with spatially variable factors such as geology, vegetation, and climate affect rates and processes of sediment transport in addition to LWD. To study the relationship between LWD, discharge, and the formation of FGCM deposits, a physical model was used to limit variability of these factors and other stream components.

Experiments were conducted in a laboratory setting to monitor how FGCM deposits form downstream of LWD under different flow conditions. The experiment

conditions were based off field conditions in the South River. Three simulations were carried out in a recirculating flume at John Hopkins University (Baltimore, MD) where discharge ranged between 0.017 m^3/s and 0.031 m^3/s but was held constant for a given run.

2.2 Physical Model Scaling

Physical models are generally scaled by size or by force, or by a combination of both. Geometric scaling is a scaling process in which all variables that have units of length are scaled by the same factor to maintain the same size ratios of features in prototype and model. Force similitude scaling seeks to maintain similar force conditions in prototype and model through a series of dimensionless parameters. Dimensionless numbers including Froude (Fr), flow Reynolds (Re), particle Reynolds (Re_p), Rouse, and Shield (τ_*) numbers, were calculated for these experiments to compare the force conditions between the model and the prototype.

In ideal models, all variables would be perfectly scaled to the model; however, in most experiments, these expectations cannot be met. Distorted Froude scale modelling (FSM) is a physical modelling approach that aims to achieve geometric, kinematic, and dynamic similarity between model and prototype while allowing flexibility in scaling parameters (Peakall et al., 1996). Distorted FSM is used to model large prototypes, such as rivers, at small scales. In this method, the geometric scale is often distorted by an increase in the vertical:horizontal ratio. Additionally the slope is steepened. The changes in the geometric scale allow for precise modelling of sediment transport. In distorted FSM, the particle Reynolds number is relaxed in turbulent flow regimes while the Froude number is scaled appropriately for the model to best maintain dynamic and kinematic similitude between model and prototype.

The physical modeling approach for the experiments utilized a distorted FSM method for a general model of fine-grained sediment transport with large bank roughness in a typical gravel-bed river.

2.2.1 Dimensionless Numbers

Each dimensionless number characterizes a different aspect of the flow to ensure model and prototype similarity. The Froude and Reynolds numbers are the ratio of inertial forces to the gravitational force and viscous forces respectively. The flow Reynolds number is used to determine if flow is turbulent, laminar or transitional. For the conditions of the South River and the experimental channel, flow should be turbulent. The particle Reynolds number documents that the flow is rough. In fully rough flows, the viscous sub-layer is contained within the unevenness of the bed. Thus, the friction becomes dependent on the roughness rather than the viscosity. The Rouse and Shields numbers are parameters of sediment transport that can be scaled from model to prototype. The Rouse number is the ratio of particle settling velocity to the shear velocity while the Shields number is the ratio of the drag force to the submerged weight of a particle. The dimensionless numbers are defined below:

Froude number $$F_r = \frac{u_0}{\sqrt{gD}}$$ (Equation 2.1)

Channel Reynolds number $$Re = \frac{u_o D}{\nu}$$ (Equation 2.3)

Particle Reynolds number $$Re_p = \frac{u_* D_{50}}{\nu}$$ (Equation 2.4)

Rouse number $$Rouse = \frac{w_s}{k u_*}$$ (Equation 2.5)

Shields number $$\tau_* = \frac{\tau_b}{(\rho_s - \rho) g D_{50}}$$ (Equation 2.6)

Relative Roughness $\frac{depth}{D_{50}}$ (Equation 2.7)

Where the following variables are defined as:

u_0 Characteristic (average upstream) flow velocity $[\frac{m}{s}]$

$u_0 = \frac{1}{N} D^{\frac{2}{3}} S^{\frac{1}{2}}$

N Manning's roughness constant

N = 0.03 for South River

g Gravitational constant $[\frac{m}{s^2}]$

D Water depth $[m]$

D_{50} Median sediment diameter $[m]$

D_{50} = 0.125 mm for South River Sand

D_{50} = 25.5 mm for South River bed sediment

ν Kinematic viscosity $[\frac{m^2}{s}]$;

$\nu = 1.0 * 10^{-6} \frac{m^2}{s}$ for fresh clear water at 20℃

w_s Fall velocity $[\frac{m}{s}]$;

$w_s = 112 \frac{mm}{s}$ for South River sand

$w_s = 479 \frac{mm}{s}$ for South River bed sediment

k Von Karman's constant

k = 0.4

u_* Shear velocity $[\frac{m}{s}]$

$$u_* = \sqrt{\frac{\tau_0}{\rho}} = \sqrt{gDS}$$

τ_* Shields number

τ_0 Boundary shear stress $[Pa]$

$$\tau_0 = \rho g D S$$

S Slope

S = 0.0013 for South River

ρ Fluid density $[\frac{kg}{m^3}]$

$\rho = 1000\ \frac{kg}{m^3}$ for clear water at 20℃

ρ_s Sediment density $[\frac{kg}{m^3}]$

$\rho_s = 2650\ \frac{kg}{m^3}$ for quartz

2.3 Experimental Scaling Conditions

The experiment conditions and model set up were based off previous field work of the South River. A diagram of a typical FGCM (Figure 2.1) deposit found in South River was the prototype for the model.

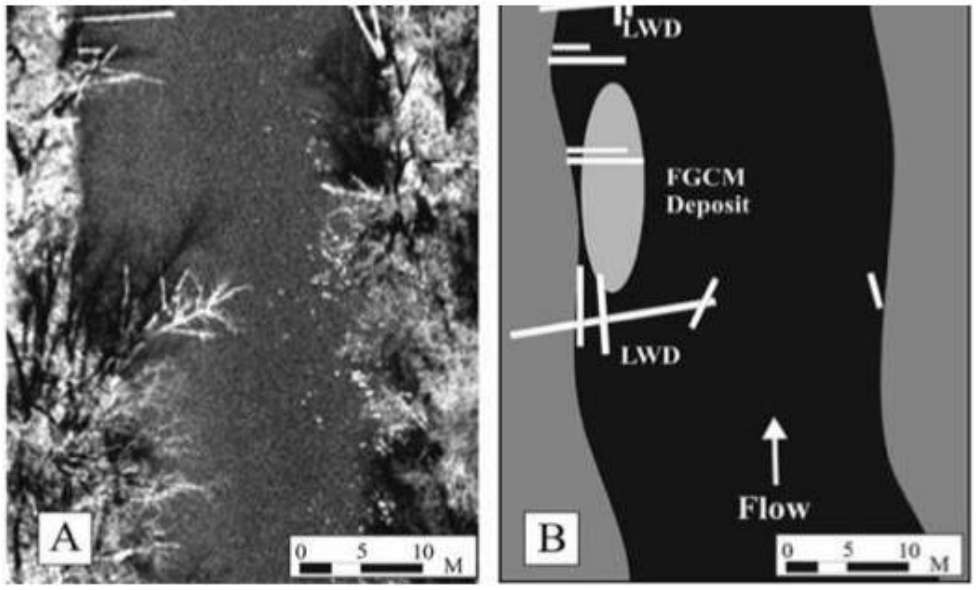

Figure 2.1: An aerial photograph of a typical FGCM deposit (Figure A) and a corresponding diagram of the same deposit (Figure B) (Skalak, 2009; Figure 4.2).

2.3.1 South River Geometry and Variables of Length Scale

The average channel width in the prototype is 22.5 m. The deposit is 5 m wide, 10 m long, and has a maximum thickness of 0.8 m. Only the first LWD was modelled in experiments. The width of this LWD piece was 11 m. The length of the two LWD pieces overlapping the first LWD piece are 6.5 in length. Average South River values and prototype values are summarized in Table 2.1.

Table 2.1 Summary of South River geometry for the model prototype and average South River conditions

Property	**South River Prototype Conditions (m)**	**South River Average Conditions (m)**
Channel width	22.5	30
Channel depth	1	1.5
LWD length across channel	11	5.6
LWD diameter	N/A	0.32
Deposit width	5	5
Deposit length	10	25
Deposit thickness	0.8	0.34
Bed sediment median diameter	0.0255	0.0255
Suspended sediment median diameter	$1.25 \cdot 10^{-5}$	$1.25 \cdot 10^{-5}$

2.3.2 South River Hydraulic Forces

Gravel-bed rivers typically have subcritical flow and transport bed load in addition to the suspended load. For these conditions, the model is expected to have a Froude number less than one. The channel Reynolds number should be greater than 500 for open channel flow and the particle Reynolds number greater than 15. Based on the hydraulic conditions of South River, the Froude number for the system is 0.41 at bankfull depth and is 0.38 at a river depth of 1 m (Table 2.2). The flow Reynolds

number is $2.36 \bullet 10^6$ and $1.20 \bullet 10^6$ for channel depths of 1.5 m and 1 m, respectively. The particle Reynolds numbers for both channel depths are greater than 15 for both conditions.

The Rouse number should be greater than 2.5 to indicate bed load transport. A rouse number less than 0.8 would indicate washload transport. For gravel-bed rivers, the Shields number is typically between 0.01 and 0.1. The Rouse number for bed load at bankfull depth and below bankfull depth are both greater than 2.5 with values of 8.66 and 10.1. The Rouse numbers for suspended sediment at or below 0.8 indicating wash load transport of fine sand. The Shields number for suspended sediment is greater than 0.1 which implies that the fine sediment is easily moved in the system. The Shields number for the bed load is 0.05 and 0.03 for bankfull and below bankfull depths. These values indicate transport of the bed sediment.

Table 2.2 Dimensionless number parameters for the South River and the equivalent expected condition for the physical model.

Dimensionless Number	**South River Conditions at Bankfull (Depth = 1.5 m)**	**South River Conditions at Below Bankfull (Depth = 1 m)**	**Expected Conditions**
Froude	0.41	0.38	< 1
Flow Reynolds	$2.36 \bullet 10^6$	$1.20 \bullet 10^6$	> 500
Particle Reynolds	$3.5 \bullet 10^3$	$2.8 \bullet 10^3$	> 15
Rouse: Sand	0.65	0.8	< 0.8
Rouse: Bed	8.7	11	> 2.5
Shields: Sand	12.7	8.5	> 0.1
Shields: bed	0.05	0.03	0.01 – 0.1
Relative Roughness: bed	59	39	-

2.4 Description of Experimental Equipment and Material

2.4.1 Hydraulic Flume

The experiments were conducted in a 14 m long, 0.6 m wide flume in which water and sediment were recirculated (Figure 2.2). Centrifugal pumps moved water from the tailbox at the downstream end through a 20 cm pipe to the upstream end of the flume (Wilcock et. al 2001). Two LWD structures were placed on opposite walls of the flume at 6.4 m and 10.0 m downstream (Figure 2.2, Figure 2.3) to serve as obstructions to the sediment circulated through the system. The slope was fixed to 0.0067 for all experiments. A right-handed coordinate system was used to refer to locations in the flume, with *X* measured in the downstream direction, *Y* measured across the flume, and *Z* measured as the elevation relative to the bed surface.

Figure 2.2 Photograph of the hydraulic flume used for the experiments. Flow directions and LWD locations are marked on the photograph.

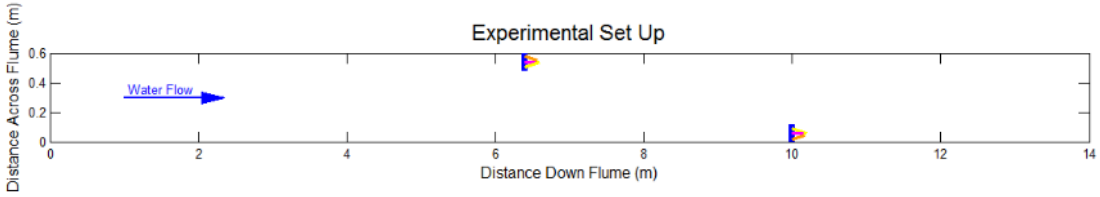

Figure 2.3: Diagram of the flume arrangement from a top-down viewpoint. LWD structures were located at 6.3 and 10.0 m downstream. Flow direction is indicated by the blue arrow. The first meter of the flume bed was a roughened reach to promote turbulent flow. The remainder of the flume bed was a fixed pebble bed. The *y* axis (distance across flume) is vertically exaggerated by a factor of 2.

2.4.2 Bed and Suspended Sediment

The flume bed was a fixed pebble surface with a D_{50} of diamater 4.5 mm (Figure 2.4), to simulate the roughness of gravel bed conditions. The bed was fixed to negate the complexities of a movable gravel bed. The pebble surface D_{84} and D_{16} values are 7.8 and 2.25 mm respectively (Table 2.2). The graphic standard deviation, also known as the sorting coefficient, of the bed sediment was 2.71 mm with a skewness of 0.22.

Suspended sediment introduced to the system was a fine sand with D_{50} of diameter 0.10 mm (Figure 2.4). The D_{84} and D_{16} values of the suspended sediment are 0.13 and 0.072 mm respectively (Table 2.3). The graphic standard deviation was 0.03 mm with a skewness of 0.18.

Table 2.3: Sorting value of pebble bed and suspended sediment.

Sorting Value	Pebble Bed	Suspended Sediment
D_{50} (mm)	4.5	0.10
D_{84} (mm)	7.8	0.13
D_{16} (mm)	2.25	0.072
Graphic mean (mm)	4.85	0.10
Skewness (dimensionless)	0.22	0.18
Kurtosis (dimensionless)	1.38	0.96
Sorting coefficient (dimensionless)	1.29	1.25

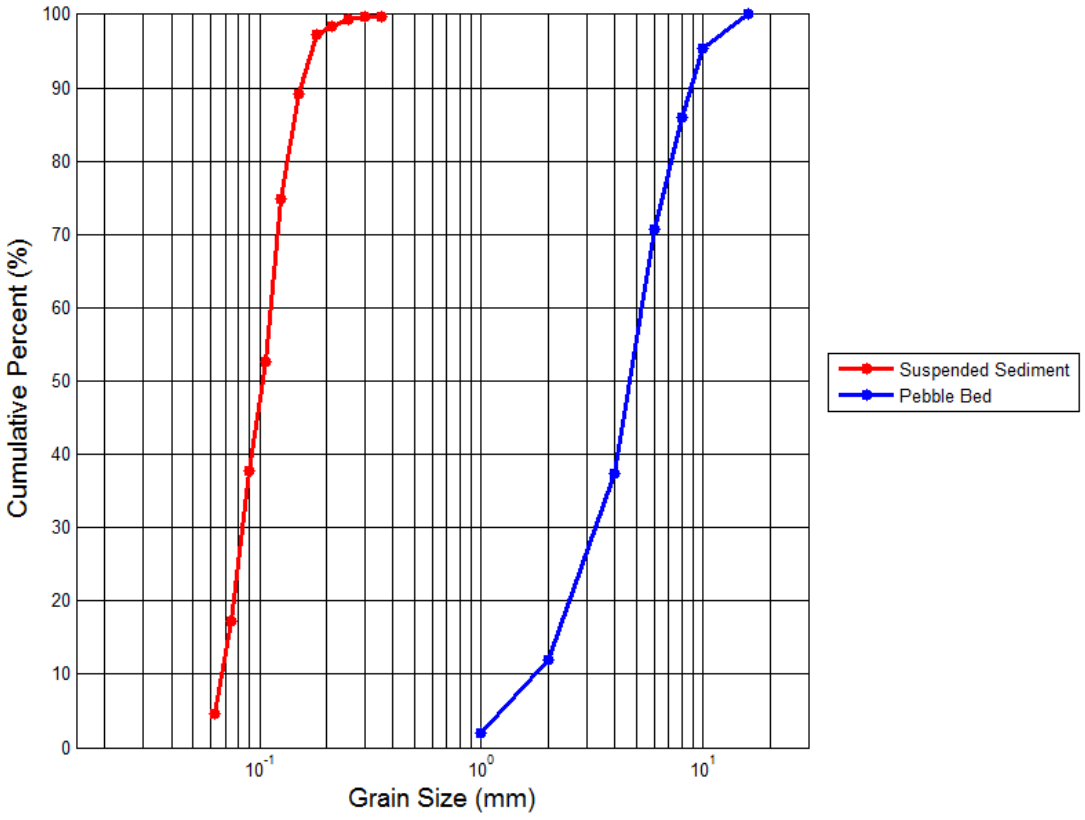

Figure 2.4: Cumulative grain size distribution of sediment in the pebble bed and suspended sediment.

2.4.3 Large Woody Debris Structures

Two LWD structures were placed on opposite walls of the flume at 6.4 m and 10.0 m downstream (Figure 2.3). The LWD structures (Figure 2.5) within the flume consist of wooden dowels, scaled using the FSM approach, and attached to the bed to prevent the structure from floating downstream. Three wooden dowels simulated the trunk of the LWD. The dowels ranged in length from 0.15 m to 0.19 m and 0.01 to 0.015 m in diameter. A wire mesh base and perforated foam pad were attached to the upstream end of the structure to simulate the rootwad of the LWD. The mesh base is 0.12 m wide and 0.15 m tall with square openings that were 0.002 m wide. A semi-permeable foam pad, 0.075 m in width and 0.15 m in height, with smaller and fewer openings was placed on the upstream end of the LWD structure obstructing about half of the mesh base. The foam pad was located closer to the channel center than the channel walls. Blue wiry mesh was also attached to the base mesh to simulate leaves and twigs that collect in the rootwad. The LWD allows sediment to move through the obstruction as well as around it.

Each LWD structure was attached to the flume wall to model LWD on the channel margins similar to field conditions. LWD within South River mainly occur along channel margins as isolated deposits, with occasional small jams of less than 5 pieces of wood. Most LWD is less than 10 m in length and all pieces are less than the average channel width of 20 - 40 m. The diameters of the LWD pieces were under 0.40 m, averaging 0.32 m. The average of LWD pieces within these deposits is 5.6 m in length.

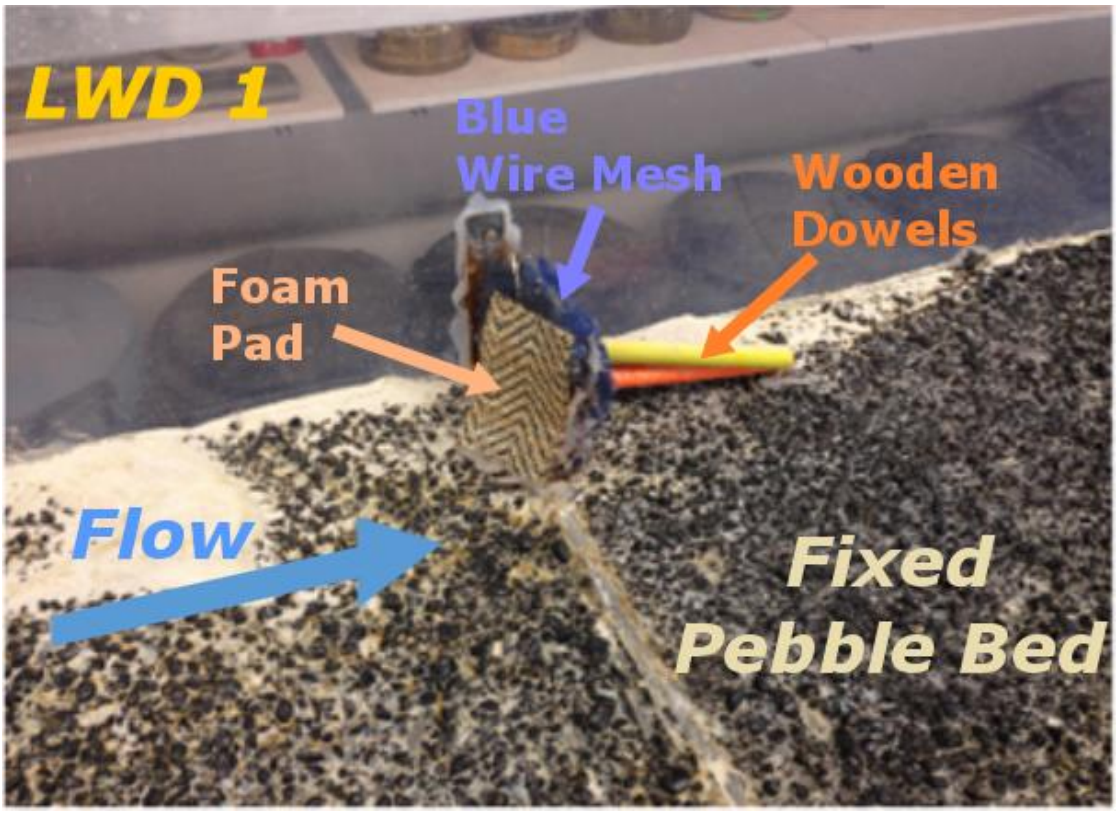

Figure 2.5: LWD structure attached to flume wall at 6.3 m downstream. The wire mesh and perforated foam pad simulate an upstream facing rootwad. The three wooden dowels simulate the trunk of the LWD.

2.4.4 Acoustic Doppler Velocimeters

Flow measurements were acquired from three Vectrino II Acoustic Doppler Profiling Velocimeters (ADPVs), which measure velocity using acoustic signals that reflect off particles in the water. The ADPV measures three components of velocity (*u*, *v*, *w*) over a 0.031 m vertical range at 0.001 m bins. The velocity components *u*, *v*, and *w* represent velocity components measured in in the *X*, *Y*, and *Z* direction respectively. The measurements were collected 0.04 m to 0.07 m from the ADPV head. The full 0.03 m range of measurements may not be fully sampled depending on the submerged depth of the Vectrino head. If the Vectrino head is less than 0.07 m above the bed, the

whole range will be sampled but a portion of the data will be false data since it falls below the bed.

The three ADPVS, spaced 0.1 m apart, sampled 6 locations (0.05-0.55 m) across the stream in two sections (Figure 2.6). The first three measurements were taken at 0.5, 0.15, and 0.25 m across flume. Then the ADPVs were moved to record a second set of three measurements at 0.35, 0.45, and 0.55 m. The 0.6 m cross-stream transect was repeated in the downstream direction every 0.5 m from 4 m to 9 m except near LWD where transects were taken at 6.3 m and 6.7 m, upstream and downstream of LWD respectively (Figure 2.7). The grid of sampling points was chosen to sample upstream, downstream, and near the first LWD obstruction. Transects before 4 m and after 9 m downstream were not sampled due to time constraints. Locations across the flume were chosen to gather the most points in the cross-stream transect most efficiently using three ADPVs while the three samplers were fixed 0.1 m apart. Each location was sampled for 8 minutes. Experimental data used for this paper were collected on a separate day from deposit measurements due to a device malfunction during the first stage of all three experimental runs.

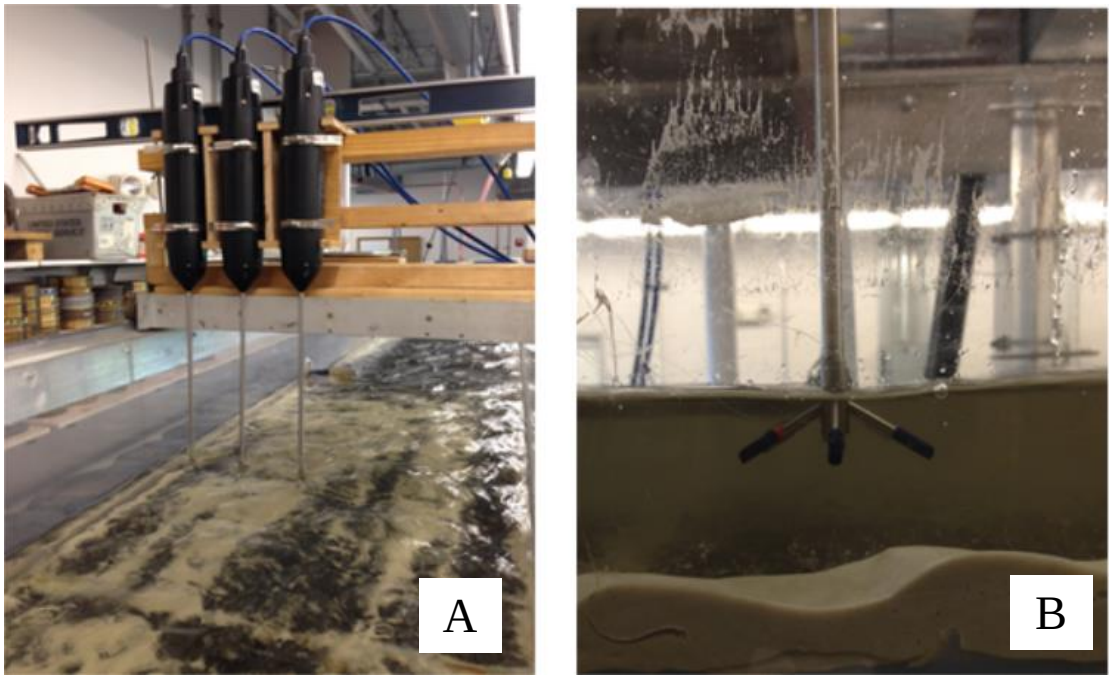

Figure 2.6: Experimental setup of 3 Vectrino ADPVs (Figure 2.5a). A Vectrino ADPV (Figure 2.5b) has four receivers that listen for the sound return of an acoustic signal sent out by the center beam. The sensor must be a minimum of 0.04 m above the bed to collect data.

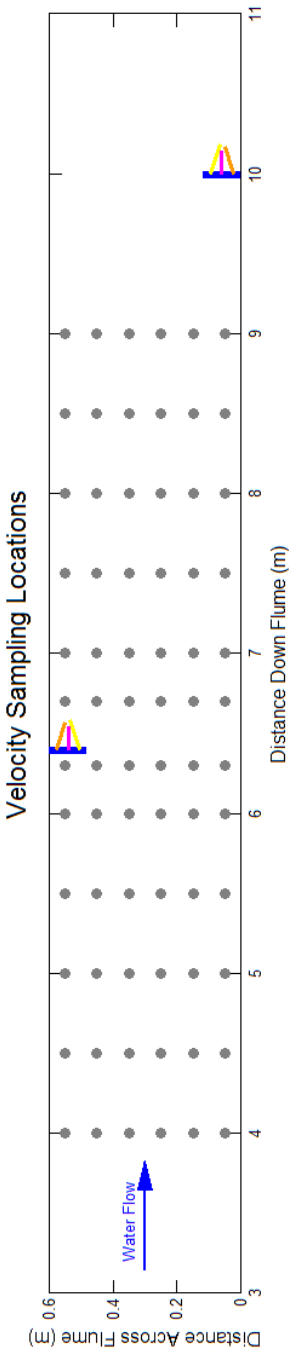

Figure 2.7 Sampling locations for velocity measurements acquired using three Vectrino ADPVs. The Y Axis is vertically exaggerated by 2.

2.4.4.1 Post Processing of Velocity Data

Acoustic Doppler instruments measure velocity with high spatio-temporal resolution. However, the precision of these sensors can be affected by Doppler noise, random spikes, bubbles, aliasing and other issues. Data from the ADPV sensors were post-processed to remove data that were influenced by the above factors.

A three-step technique was applied to the data to remove spikes, data with poor correlation, and data apparently obtained below the physical bed. Data points were retained when the instantaneous correlation value (averaged over the four beams) was greater than 75%. Data were also passed through a phase despiker (code written by Nobuhito Mori) to remove spikes and outliers. Lastly, all data below the bed were removed. The bed was defined as the bin where the velocity was less than 0.03 m/s and the standard deviation was less than 0.05.

2.5 Experimental Procedure

Each Experiment consisted of five stages: flume preparation, hydraulic measurements, initial deposit measurements, sediment addition, and final deposit measurements. Three experiments were run following the same procedure, but each at different discharge to determine the effects of flow on deposit formation. The experiments will be referred to Low Flow (LF), Medium Flow (MF), and High Flow (HF).

In the first stage, the flume channel was prepared for experiments by removing the majority of sand present in the channel from previous testing. The sand was removed by scooping and vacuuming sand out of the channel. Due to the roughened bed surface, not all sand could be removed because it would settle in crevices. Sand

would also remain in the pipes that brought water and sand from the flume tailbox to the main channel. The sand that could not be removed from the channel was assumed to have minimal effect on velocity measurements. The remaining sand would be accounted for in the initial measurements of the deposits.

After sand was removed, hydraulic conditions were then recorded. In this stage, water was introduced to the channel and run continuously. Water was run at a constant rate for each experiment. The flow rates for Experiment LF, Experiment MF, and Experiment HF were 0.017, 0.025, and 0.031 m^3/s respectively. Flow depth was measured with a point gauge while velocity measurements were recorded by ADPVs. Hydraulic measurements were taken with minimal sand in the channel because of concerns that the Vectrino probe heads would disturb the deposit evolution when sand was present in the channel.

While the water was running, the sediment that could not be removed would build a deposit downstream of the wood. After all velocity measurements were taken, water was turned off. No visual changes to the deposit topography were seen when the water was drained from the channel, but measurements were not made to confirm this observation. The deposit that was established during this stage is classified as the base deposit. This initial deposit was comparable in width and length to the final deposit but the height was less. Deposit growth was measured from this initial formation.

Initial deposit size was measured in the third stage. The width, length, and height of the base deposit were measured. The width was measured every 0.05 m for the entire length of the deposit. The height was measured using a point gauge to mark the top of the deposit and the top of the pebble bed every 0.05 m for 1 m downstream

from the start of the deposit in two downstream transects spaced approximately 0.02 m apart in the cross stream direction.

After deposit size was measured, sediment was introduced to the flow to provide the sediment supply to monitor how the deposits evolved. Water was turned on and flow was reintroduced to the channel. Approximately 18 L, or 18 kg, of sand were introduced during each experiment through a tailbox at the end of the flume. Sediment was added while flow was being pumped through the channel so that flow would mix the sediment with the water in the tailbox before being introduced to the channel at the upstream end. Hydraulic measurements were not taken during this stage to allow the sediment to flow without any interference from the ADPV equipment to document deposit growth typically seen in the field. Water was run during this stage for each experiment for about 3 hours to attain a steady-state configuration, identified by constant morphological conditions of the FGCM deposits. Equilibrium of deposit topography was identified visually.

Once an equilibrium deposit had formed, water was turned off and width, length, and height of the deposit were measured again. The measurements were conducted in the same way as the third stage.

Chapter 3

RESULTS

3.1 Hydraulic Conditions

Three experiments were run at discharges of 0.017, 0.025, and 0.031 m^3/s. The hydraulic conditions for all experiments are summarized in Table 3.1. Water depths for all experiments are shown in Figure 3.1. In all experiments, water pooled upstream of the wood structure located at 6.3 m downstream. The pool extended from the 2 m mark to the wood obstruction. After each wood obstruction was a shallow section across the entire channel for about 2 m in the downstream direction. The shallow section was most prominent on the opposite side of the channel from the LWD. The water was most shallow on the opposite side of the channel from the LWD. Water downstream of the first LWD obstruction increased in depth at 8 m. This depth may be influenced by the presence of an LWD structure at 10 m creating another pooling effect. The change in velocities near the wood will be discussed in a later section

Experiment LF was run at a discharge of 0.017 m^3/s. The average upstream velocity was 0.33 m/s and the average upstream depth was 7.6 cm. The water temperature for this experiment was 20.6℃.

Experiment MF was run at a discharge of 0.025 m^3/s. The average upstream velocity was 0.39 m/s and the average upstream depth was 8.5 cm. The average water temperature for this experiment was 24℃.

Experiment HF was run at a discharge of 0.031 m^3/s. The average upstream velocity was 0.40 m/s and the average upstream depth was 8.7 cm. The average water temperature for this experiment was 21.1℃.

Table 3.1 Summary of the hydraulic conditions of all experiments

Hydraulic Condition	**Experiment LF**	**Experiment MF**	**Experiment HF**
Discharge (m^3/s)	0.017	0.025	0.031
Velocity (m/s)	0.33	0.39	0.40
Temperature (C)	20.6	24	21.1
Average upstream depth (m)	0.076	0.085	0.087

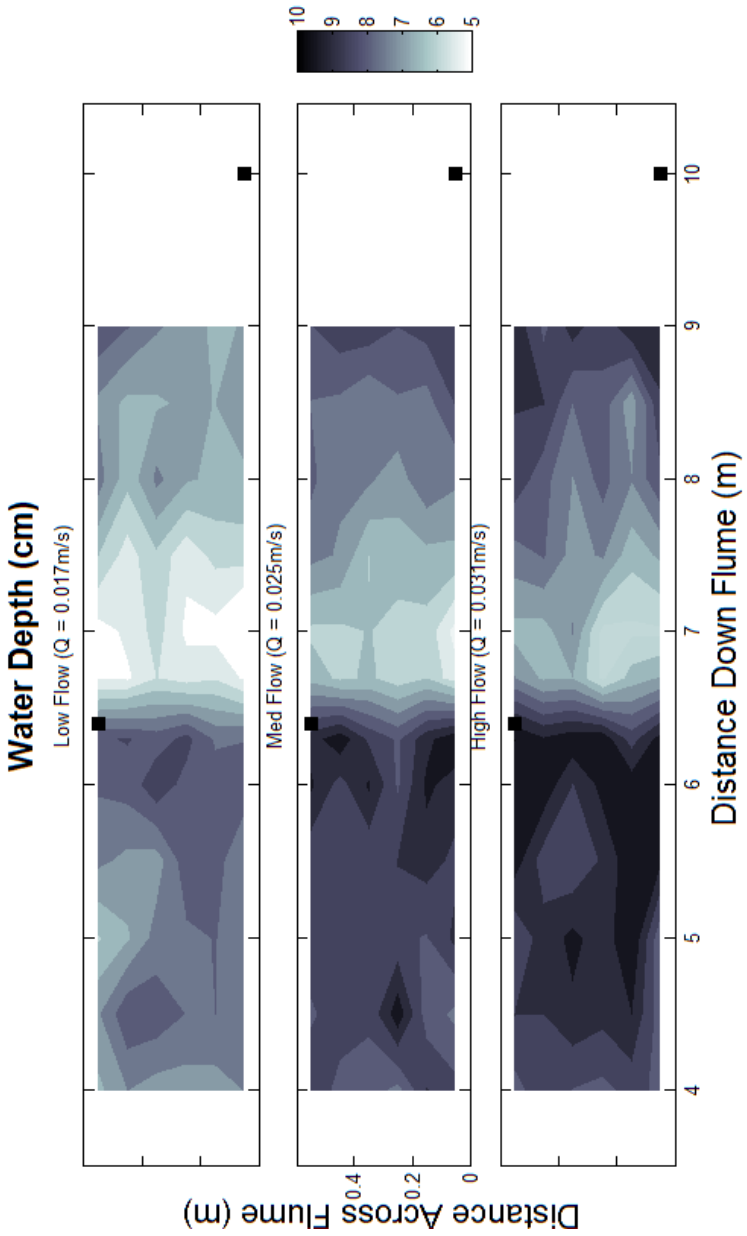

Figure 3.1 Water depths for each experiment. Water pooled upstream of the wood obstruction located at 6.3 m downstream. The water became shallow near the wood, especially on the opposite side of the channel. Water began to deepen again at about 8 m due to the second wood obstruction located at 10 m downstream.

3.2 Velocity Data Post Processing

Data was cleaned using a post processing script to remove false or poor data from the Vectrino files. An example of the post processing data removal is shown in Figure 3.2. The velocity, shown along the x axis, is plotted against the bin number along the y axis. Bin 31 is closest to the sensor head (4 cm away from sensor head) while bin 1 is the farthest (7 cm away from sensor head). Raw data is shown in black. The red data, which encompasses the green section and the red, is all the data that remained after spikes were removed. The blue line is what is identified as the bed of the channel, all data below this point was removed. The green data shows all data kept after poor correlations were removed as well as data below the bed.

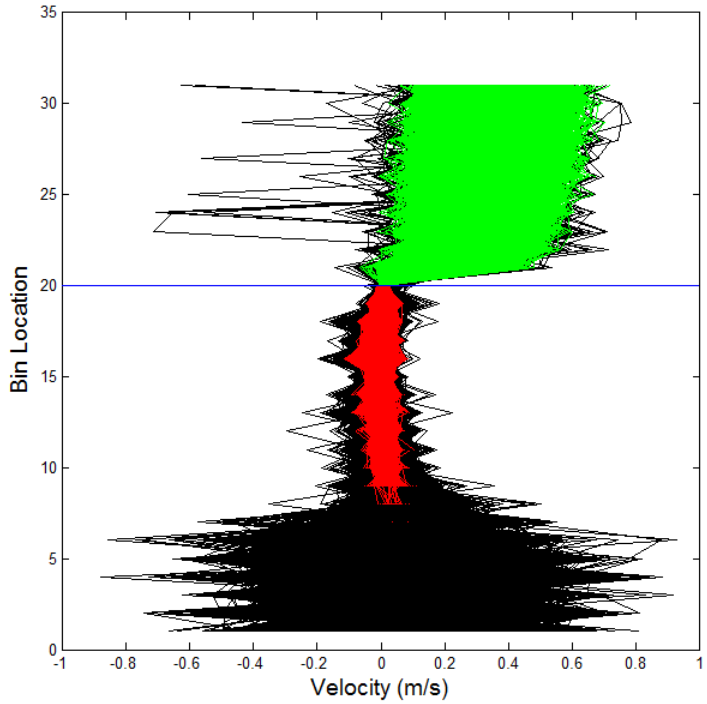

Figure 3.2 An example result of processing of Vectrino raw data.

3.3 Velocity

Velocity from the remaining accepted ADPV data was used to map the flow field in the region surrounding the first LWD obstruction (Figure 3.3). The flow maps show how the water is moved around the wood creating a region of low velocity downstream of the wood. Velocities for the vector fields and discussed in this section are averaged over the top three bins near the sensor head. Velocities near bed are ignored since they approach zero and skew the mean. Near bed velocities were used to calculate boundary shear stress, which will be discussed in a later section. The flow maps show velocity in the X and Y directions. Positive velocities in the X direction indicate downstream flow while negative values indicate upstream flow. Positive velocities in the Y direction indicate flow to river left, looking downstream.

In all experiments, the water upstream of the wood approaches flowing almost mainly in the downstream direction with minimal flow in the cross-stream Y and the vertical Z direction. As the water nears the wood, the flow shifts towards the river right wall of the channel. After the water passes the wood, a portion of water flows back downstream of the wood and reestablishes a slower flow. The water in the center of the channel reestablishes a straight flow and begins to slow as it approaches the second LWD obstruction.

In Experiment LF, the average upstream velocity is 0.33 m/s in the downstream X direction, -0.003 m/s in the Y direction, and -0.020 m/s in the Z direction. In the sampling transect at 6.3 m downstream, the flow slows directly in front of the wood (0.55 m across flume). The velocity was measured to be 0.13 m/s in the X direction and -0.07 m/s in the Y direction. On the same transect, at 0.45 m and 0.35 m across flume, the velocity remains primarily in the downstream direction with speeds of 0.25 m/s and 0.15 m/s respectively with Y velocities of -0.22 m/s and -0.15

m/s. Along the 6.3 m transect, velocity in the Y direction increases in comparison to upstream flows, with direction advancing towards river right. Directly downstream of the wood (coordinates 6.7m, 0.55 m), velocity was measured to be 0.005 m/s in the X direction and 0.017 m/s in the y direction. This indicates a slow flow towards river left downstream of the wood. Along the 6.7 m downstream transect, velocities in the center of the channel at were 0.21 m/s, 0.14 m/s, and 0.30 m/s in the X direction at 0.45 m, 0.35 m, and 0.25 m. The corresponding Y velocities were 0 m/s, 0.05 m/s, and 0.05 m/s. Velocities measured at 0.15 m and 0.05 m along this 6.7 m transect are near zero but this may be influenced by sampling close to the bed since flow was shallow in this section.

In Experiment MF, the average upstream velocity is 0.39 m/s in the downstream X direction, -0.005 m/s in the Y direction, and -0.034 m/s in the Z direction. In the sampling transect at 6.3 m downstream, it is seen that the flow directly in front of the wood (0.55 m across flume), the velocity slows to -0.01 m/s in the X direction. On the same transect, at 0.45 m and 0.35 m across flume, the velocity remains primarily in the downstream direction with speeds of 0.35 m/s and 0.33 m/s respectively. Along the same transect, velocity in the Y direction increases in comparison to upstream flows, with direction advancing towards river right. Y velocities were measured to be -0.03 m/s, -0.045 m/s and -0.047 m/s at 0.55 m, 0.45 m and 0.35 m across channel. Directly downstream of the wood (coordinates 6.7m, 0.55 m), velocity was measured to be 0.14 m/s in the X direction and 0.031 m/s in the y direction. This indicates a slow flow towards river left downstream of the wood.

In Experiment HF, the average upstream velocity is 0.40 m/s in the downstream X direction, 0.0034 m/s in the Y direction, and -0.024 m/s in the Z

direction. In the sampling transect at 6.3 m downstream, velocity directly in front of the wood (0.55 m across flume), is 0.066 m/s in the X direction while velocities at 0.45 m and 0.35 m across flume are 0.30 m/s and 0.44 m/s respectively. Along the 6.3 m downstream transect, velocity is seen to shift to the right as it approaches the LWD structure. Y velocities were measured to be -0.04 m/s, -0.25 m/s and -0.15 m/s at 0.55 m, 0.45 m and 0.35 m across channel. Directly downstream of the wood (coordinates 6.7m, 0.55 m), velocity was measured to be -0.08 m/s in the X direction and -0.05 m/s in the y direction. The flow downstream of the wood is upstream and towards river right which reveals a circulating current.

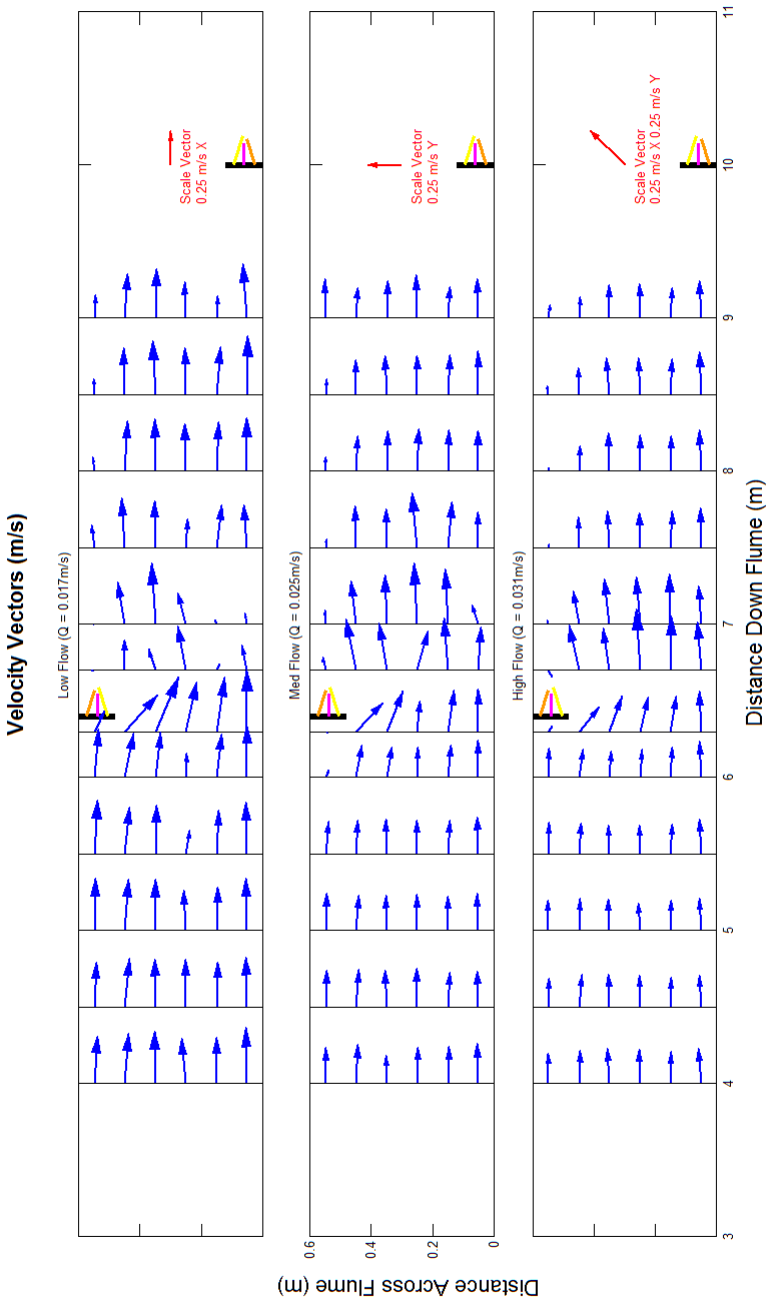

Figure 3.3 Map of velocity vectors upstream, near, and downstream of the first LWD obstruction.

3.4 Shear Stress

The boundary shear stress is a frictional force per unit area exerted on a channel boundary by the flowing water. When the shear stress exerted by the fluid exceeds the critical shear stress, the flow can initiate movement of sediment grains on the bed. In areas of high boundary shear stress, sediment will be eroded from the bed, whereas in areas of low shear stress, there will be sediment deposition. The local bed shear stress for these experiments was estimated from the Reynolds stress (Equation 3.1) and from the Turbulent Kinetic Energy (TKE) (Equation 3.2).

$$\tau_{Re} = -\rho\langle u'w'\rangle \qquad \text{(Equation 3.1)}$$

$$\tau_{TKE} = \frac{1}{2} * C_1 * \rho * \left(\langle u'u'\rangle + \langle v'v'\rangle + \langle w'w'\rangle\right) \qquad \text{(Equation 3.2)}$$

Where the following variables are defined as:

τ_{Re}	Boundary shear stress
ρ	Density of clear water at 20℃
u'	Fluctuations in the downstream velocity
v'	Fluctuations in the cross-stream velocity
w'	Fluctuations in the vertical velocity
$\langle \quad \rangle$	Time average of the product of fluctuations
C_1	Proportionality constant, $C_1 = 0.19$
τ_{TKE}	Boundary shear stress estimated from turbulence

The shear stress values were depth averaged for all velocity measurements in the velocity profile. In all experiments, τ_{Re} (Figure 3.4) and τ_{TKE} (Figure 3.5) estimated similar patterns of shear stress; however, τ_{TKE} values had a much greater range. Shear stress in the channel was low in the backwater pool upstream of the wood. High shear stress values were seen downstream of the wood from 0.25 m to 0.45 m cross-channel. An area of low shear stresses were detected downstream of the wood from 6.7 m to 9 m at 0.55 m across the channel.

The average upstream τ_{Re} values were 0.68 Pa, 0.85 Pa, and 0.77 Pa for Experiments LF, MF, and HF while τ_{TKE} values were 0.97 Pa, 1.01 Pa, and 0.97 Pa, respectively. Upstream of the wood at 0.55 m cross-stream, there was a slight increase in boundary shear stress, especially in Experiment HF. At this location, the τ_{Re} was 0.76 Pa for Experiment LF and 1.92 Pa for Experiment HF. Experiment MF had a negative shear value, which is not a valid measure. The τ_{TKE} values were 1.41 Pa, 1.37 Pa, and 2.34 Pa for the location directly upstream of LWD1, with values respective to experiments in order of increasing discharge.

An increase in shear values was seen in all experiments downstream of the wood at locations generally 0.25 – 0.45 m across the channel. The area of high τ_{Re} for Experiment LF is concentrated at 0.45 m cross-stream, beginning at 6.7 m downstream and stretching to 8 m downstream with some spread into the center of the channel. The τ_{Re} was greatest for Experiment LF at 6.7 m downstream, 0.45 m cross-stream with a value of 1.62 Pa. In Experiments MF and HF, the center of the region of high τ_{Re} is located farther downstream and closer to the center of the channel. For Experiments MF and HF, the τ_{Re} was greatest at 7 m downstream, 0.35 m cross-stream, with values

of 2.29 Pa and 2.66 Pa. The region of high τ_{Re} for these experiments was also seen to spread across the channel width more than the region of high shear in Experiment LF.

High τ_{TKE} values were present at 6.7 m downstream, 0.45 m cross-stream for all experiments. The τ_{TKE} values for this location decreased with increasing discharge with values of 4.93 Pa, 4.05 Pa, and 3.41 Pa for Experiments LF, MF, and HF, respectively. However, Experiment HF had the highest τ_{TKE}, 8.46 Pa, located at 7 m downstream, 0.15 m cross-stream.

An area of low boundary shear stress was seen downstream of LWD1, at 0.55 m cross-stream from 6.7 m to 9 m downstream for all experiments. For Experiment LF, τ_{Re} values ranged from $7.3 \cdot 10^{-4}$ Pa to 0.21 Pa while the τ_{TKE} values for Experiment LF ranged from $4.5 \cdot 10^{-3}$ Pa to 0.57 Pa. For both values, the lowest was located at 7 m downstream. Experiment LF had ranges of 0.07 Pa to 1.42 Pa and 0.53 to 1.56 Pa for τ_{Re} and τ_{TKE}, respectively. The highest value of the range for both shear stress estimates occurred at 9 m while the lowest value was located at 7 m and 8.5 m for τ_{Re} and τ_{TKE}. The range of shear stress values downstream of LWD1 for Experiment HF was $3.3 \cdot 10^{-3}$ Pa to 0.42 Pa for τ_{Re} and 0.21 to 1.35 Pa for τ_{TKE}. The highest shear value for both estimates occurred at 7 m. The lowest τ_{Re} in this region occurred at 6.7 m while the lowest τ_{TKE} occurred at 8.5 m.

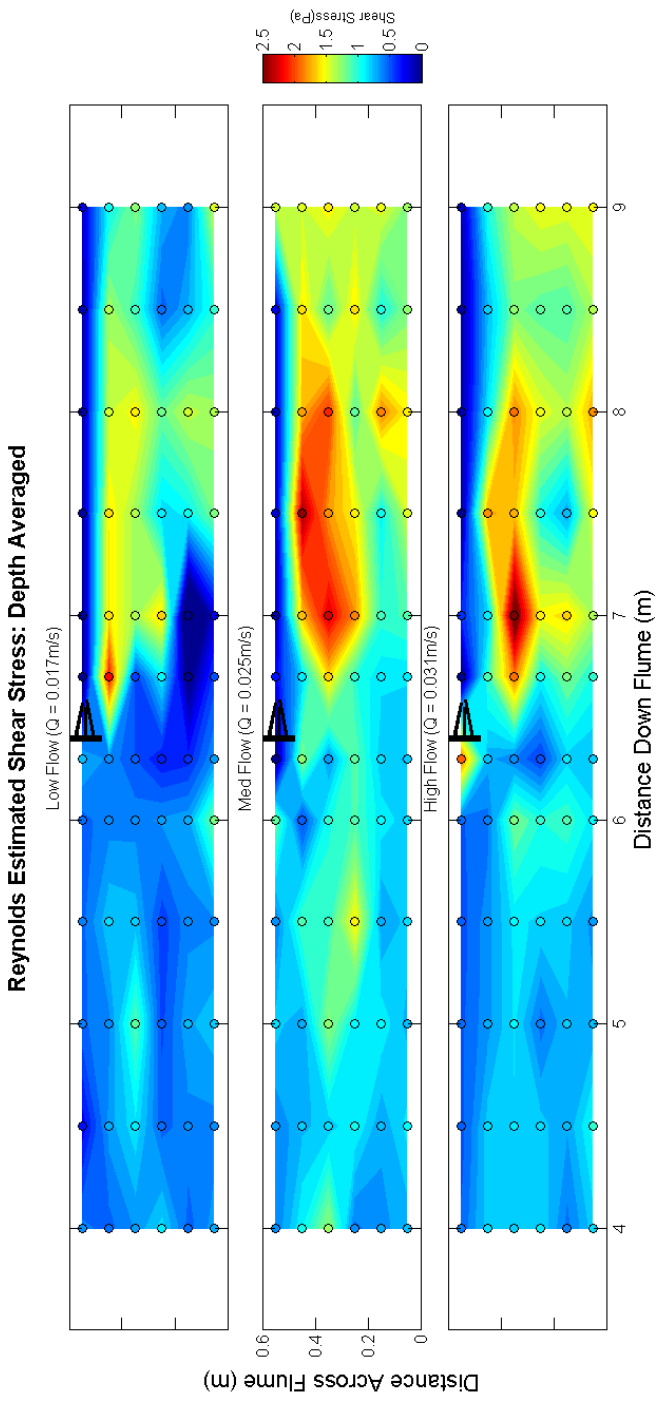

Figure 3.4 Map of shear stress values, estimated from Reynolds stresses, in the flume channel.

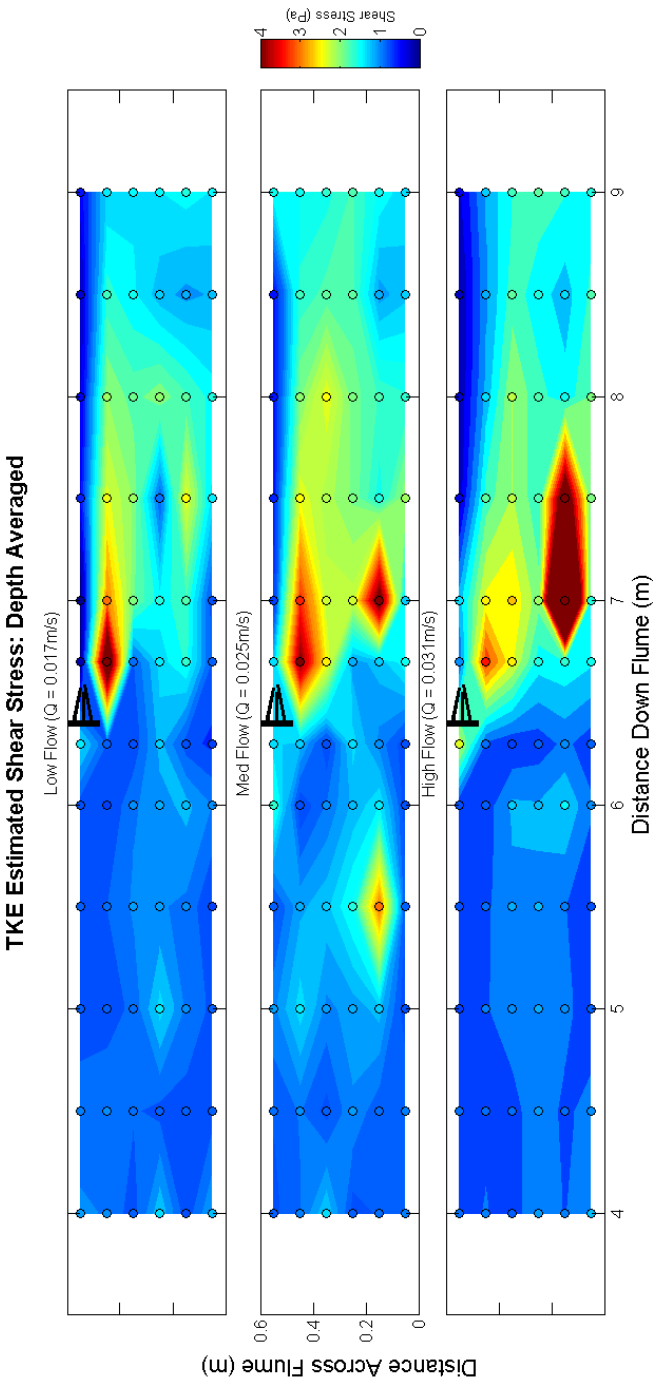

Figure 3.5 Map of shear stress values, estimated from TKE, in the flume channel.

3.4.1 Critical Shear Stress and Grain Shear Reynolds number

To determine initiation of motion for both the bed sediment and the suspended sediment, the dimensionless shear stress (τ_*) and grain shear Reynolds (Re_*) numbers were calculated. The two parameters form the Shields diagram which defines an entrainment threshold defined as the critical shear stress. If the dimensionless shear stress overcomes the critical shear stress, sediment transport occurs.

The dimensionless shear stress (Equation 3.3) is calculated using τ, the bed shear stress responsible for initiating a particle of a particle grain size. The grain shear Reynolds (Equation 3.4) is a measure of the bed roughness relative to the thickness of the viscous sub-layer. At high values of Re_*, the flow becomes fully rough and the critical shear stress becomes constant (approximately 0.056). For distorted FSM scaled models, rough flow is characterized by particle Reynolds numbers > 15 (Peakall 1996).

$$\tau_* = \frac{\tau}{(\rho_s - \rho)gD} \qquad \text{Equation (3.3)}$$

$$Re_* = \frac{u_* D}{\nu} \qquad \text{Equation (3.4)}$$

Where the following variables are defined as:

τ_*	Dimensionless shear stress
τ	Boundary shear stress
ρ_s	Sediment density
ρ	Fluid density
G	gravitational constant
D	Grain size
Re_*	Particle Reynolds number

u_* Shear velocity

v Kinematic viscosity

The dimensionless shear stress for the suspended sediment was less than 0.05 downstream of the wood for the length of the deposit for Experiment LF except at 9 m downstream where τ_* was 0.13 (Figure 3.6). In Experiment MF, one point at 7m downstream, 0.55 m cross stream had a dimensionless shear value less than 0.05 but all other values downstream of the wood ranged from 0.20 to 0.88. For experiment HF, the lowest dimensionless shear for suspended sediment downstream of the wood was 0.0020 at 6.7 m downstream, 0.55 m cross stream while the highest τ_*, 0.26, was located at 7 m downstream. All other values downstream of the wood for Experiment HF ranged from 0.015 to 0.096.

The bed sediment for all experiments experienced shear values less than 0.05 (Figure 3.7). Average upstream values of τ_* were 0.009, 0.010, and 0.010 for Experiments LF, MF, and HF. Similar to the dimensionless shear stress of the suspended sediment, an area of lower τ_* for the bed sediment developed downstream of the LWD along the channel margin.

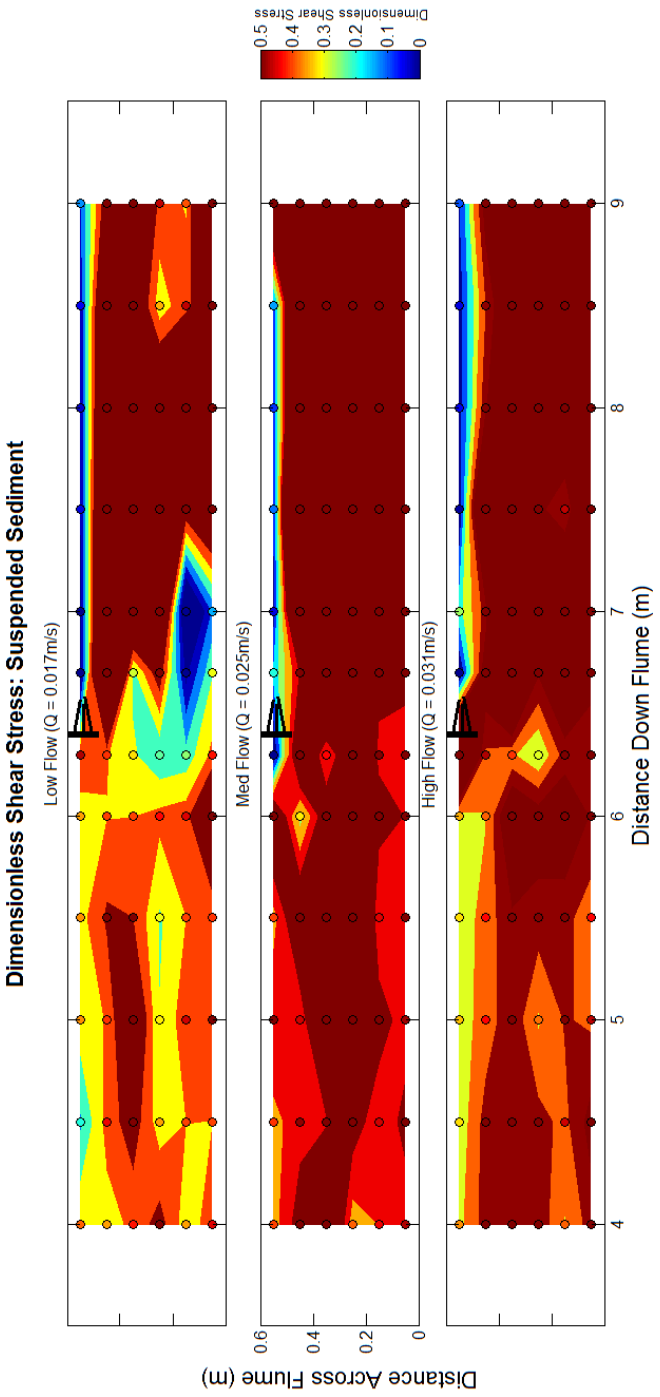

Figure 3.6 Dimensionless shear stress for suspended sediment in the flume channel.

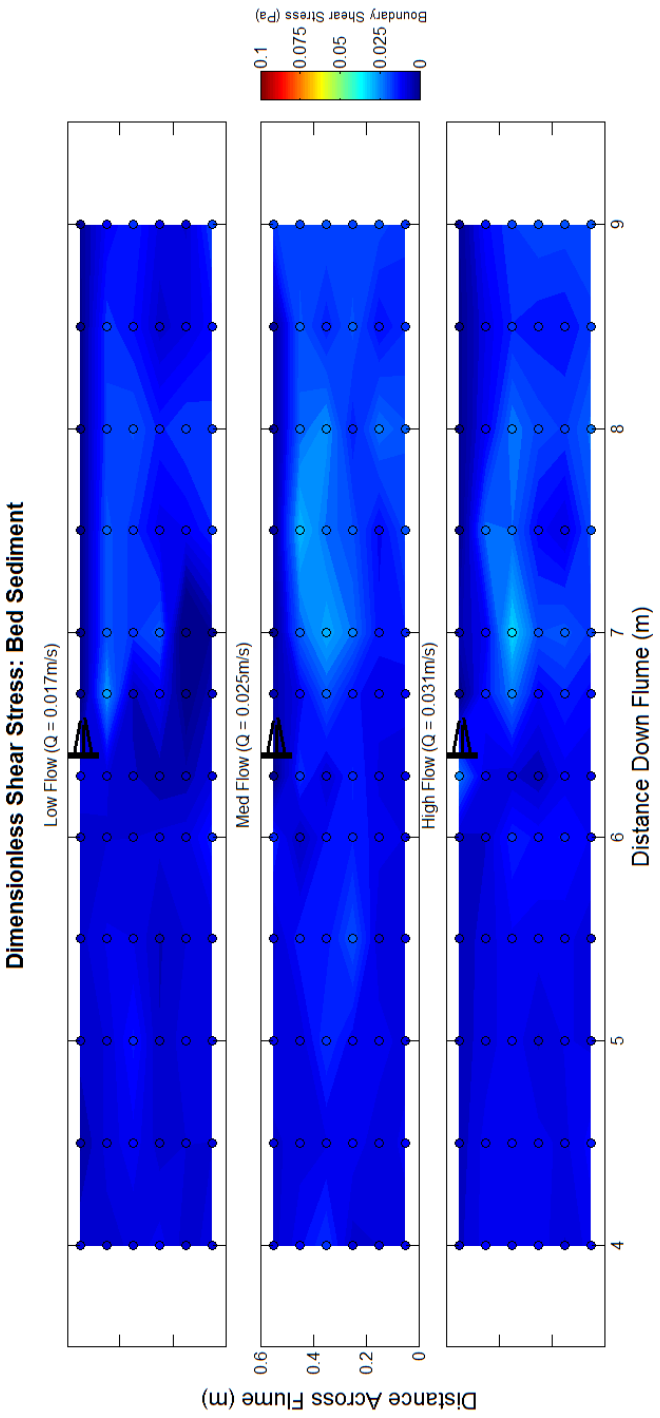

Figure 3.7 Dimensionless shear stress for the bed sediment in the flume channel.

3.5 Turbulence

TKE is a measure of the kinetic energy per unit mass. It is typically associated with eddies in turbulent flow. Fluid flowing past an object creates reverse currents and swirling of the fluid. TKE is characterized by the average of the velocity fluctuations (Equation 3.2). TKE values calculated for this study were depth-averaged.

TKE patterns were the same as TKE estimated shear stress because the estimate is a value generated from TKE. Upstream TKE values were approximately 0.01 J for all experiments with average TKE being 0.0103 J, 0.0106 J, and 0.0103 J for Experiment LF, MF, and HF (Figure 3.8). The highest TKE value (0.089 J) was detected in Experiment HF. For all experiments, there is a small increase of TKE directly upstream of the wood followed by high TKE values just downstream of the LWD at 6.7 m downstream, 0.45 m cross-stream. For Experiment HF, the TKE is 0.025 J upstream of LWD1 followed by 0.036 J downstream of the wood at 0.45 m cross-stream. Experiment MF and LF both had a smaller increase of TKE in front of the wood, 0.014 J and 0.015 J respectively, followed by greater TKE, 0.042 J and 0.052 J, downstream of the wood. High TKE values in all experiments were concentrated along the 0.35 m and 0.45 m transects from 6.7 to 8 downstream. As seen Figure 3.8, TKE was focused most narrowly in Experiment LF with high TKE values being concentrated along the 0.45 m cross stream transect. Experiment MF and Experiment HF had increased TKE spread across the channel.

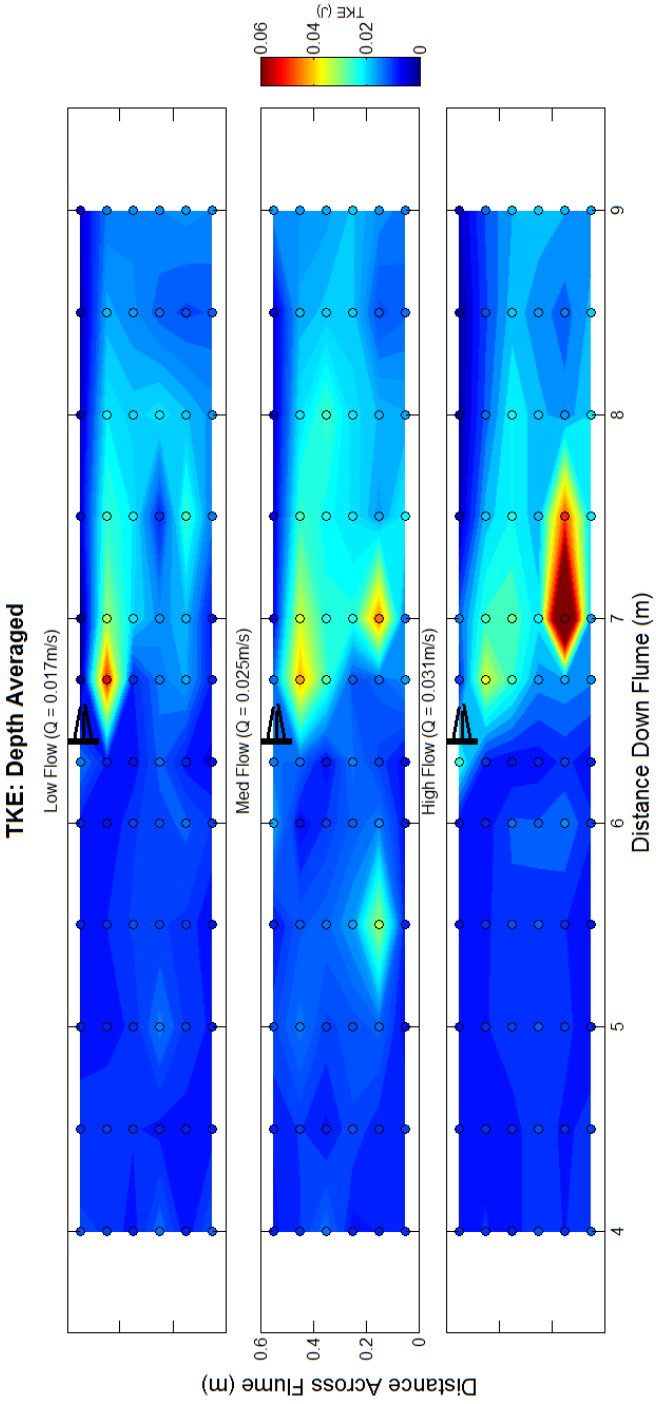

Figure 3.8 Turbulent Kinetic Energy

3.6 Sediment Concentration

Sediment concentration was tested during experiments by siphoning water and sediment from the channel into graduated cylinders. The sediment was then filtered from the water and dried in an oven. The dried sediment was used to calculate a concentration for the amount of water. This technique however resulted similar results from pre and post sediment addition to the system for each experiment. The lack of difference between stages prevents the results from being used.

Sediment concentration was calculated for the purpose of this paper by estimating the volume of water in the tailbox and the amount of sediment added to the system. For each experiment approximately 18 kg of sediment was added to the system. The tailbox holds approximately 1600 L (1.6 m^3) of water and was filled completely until excess water began to flood into the channel. The estimate of sediment concentration then is 11250 mg/L for all experiments.

3.7 Deposit Formation

Deposit formation was monitored visually during the sediment addition stage of the experimental procedure. In this stage, sediment and water were pumped through the model system for 3 hours. Sediment movement and ripple direction along the deposits were indicators of deposit formation.

For all experiments, deposits formed downstream of LWD. The length, width, and height of each deposit will be discussed in the next section. No sediment was deposited within the logs of the LWD obstruction, rather, sediment was deposited between the LWD and the channel wall and downstream of the LWD (Figure 3.9). Downstream of the LWD, a large buildup of sand was established. In this first section, the deposit exhibited downstream migrating ripples. Just downstream of the first

section of the FGCM deposit, the sand thinned and upstream migrating ripples developed (Figure 3.9). The FGCM deposits from the start of the deposit to the end of the upstream migrating dunes were about 0.25 m in length. Following the upstream migrating dunes were a second set of downstream migrating ripples. In Experiments MF and HF, a cut zone of little or no sand deposition preceded the second set of downstream migrating ripples (Figure 3.11). The deposit continued after this cut zone with deposition typically ending at approximately 10 m downstream where the second LWD obstruction was located on the opposite wall.

In visual and video monitoring, sediment movement along the deposits confirmed the ripple patterns. Downstream of the wood, sediment was seen recirculating upstream along the deposit. After the upstream migrating ripples, sediment was pushed downstream along the deposit.

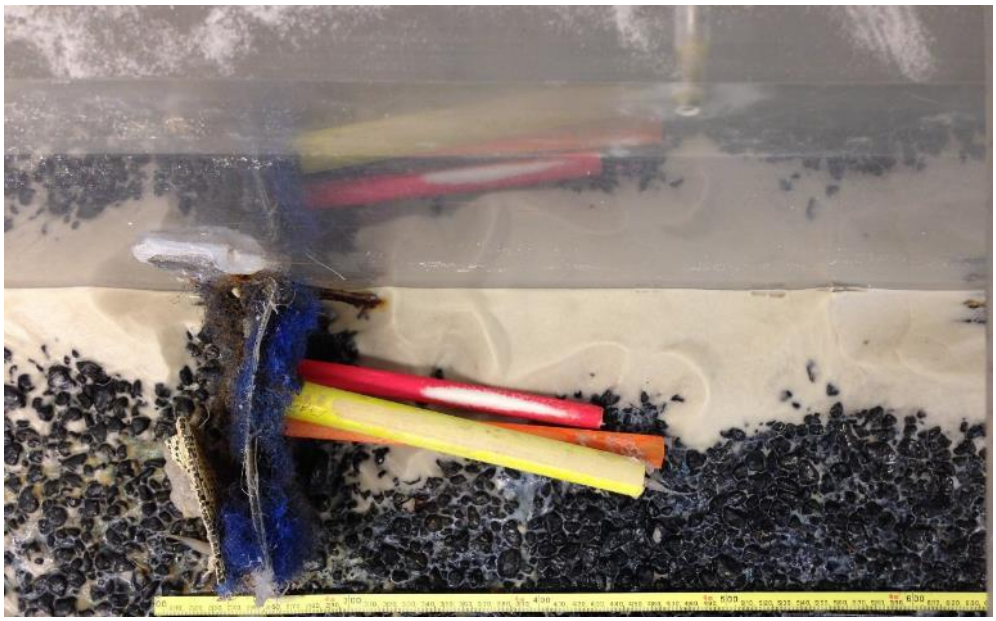

Figure 3.9 FGCM deposit downstream of the LWD. No sand is deposited within the dowels. Sand is deposited between the dowels and the channel wall as well as downstream of the LWD structure.

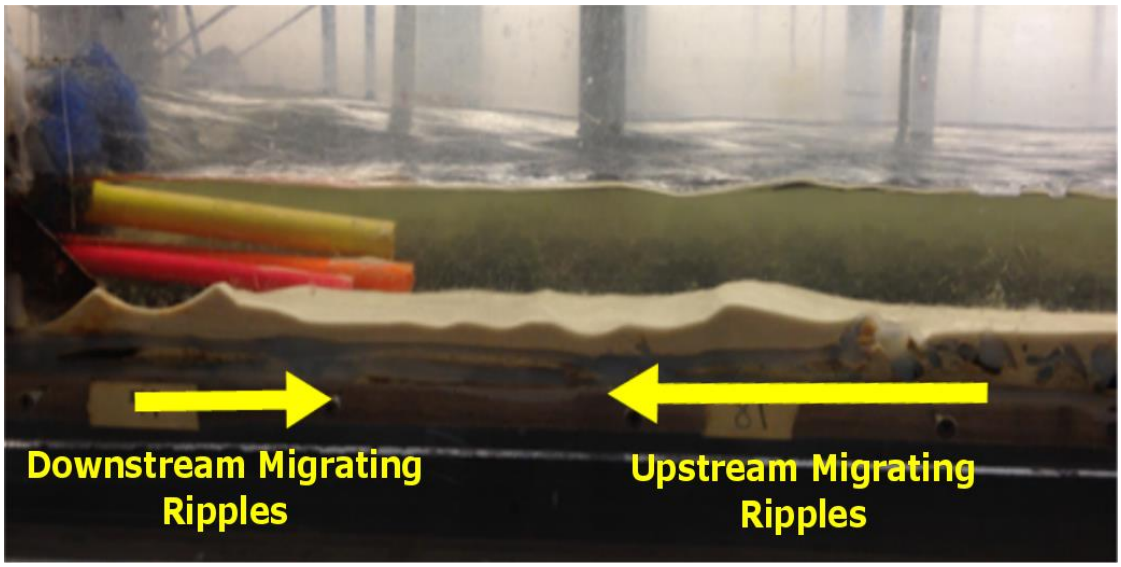

Figure 3.10 Photograph of ripples forming in FGCM deposit downstream of LWD.

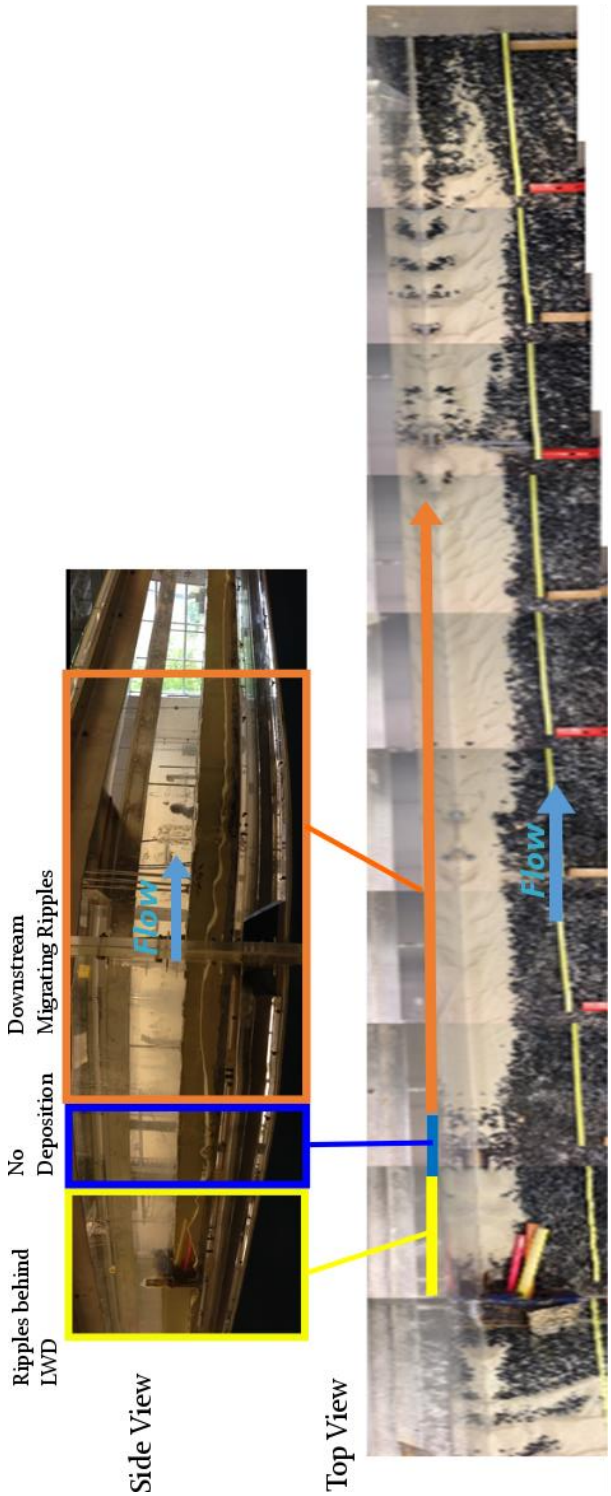

Figure 3.11 Side view and top down view of FGCM deposit. The cut zone of no sand deposition can be seen downstream of the upstream migrating ripples.

3.8 Deposit Geometry

In this section, length, width, and height of deposits will be reported for the deposits that formed downstream of each of the LWD obstructions. Continuous deposit heights were interpolated in MATLAB from two transects of sampled heights. Each interpolated point is a grid cell of length 0.5 cm and width 0.01 cm.

For this section, the first LWD at 6.3 m downstream will be referenced to as LWD1 and the second at 10 m downstream will be referenced as LWD2. The deposits corresponding to each LWD obstruction will be named FGCM1 and FGCM2. Table 3.2 and Table 3.3 summarize the average deposit geometry for each experiment, pre and post sediment addition.

The length of the deposit remained fairly consistent for each experiment pre and post sand. The length also did not vary for different flow conditions. The typical length for the deposit downstream of LWD1 was about 3.4 m. The deposit began downstream of LWD1 typically at about 6.45 m downstream. The deposit continued until about 10 m downstream which is where the LWD2 was located on the opposite wall. The length for FGCM2 for all experiments was about 1.1 m except for Experiment LF post sand which had a length of 0.85 m. The deposit downstream of LWD2 typically ended where water depth became shallow as it began to near the end of the channel.

Unlike the length, the width of the deposits varied across experiments. FGCM1 was widest for the high flow discharge conditions with a pre sand average width of 0.088 m and a post sand average width of 0.107 m. The deposit was most narrow for Experiment MF with average widths of 0.072 m and 0.088 m during pre and post sand conditions, respectively. The average width for FGCM1 increased with the addition of sand for all experiments. The maximum width for the FGCM1 was consistent for

Experiment LF pre and post sand addition but increased for Experiment MF and HF after sand was added to the channel. FGCM2 had similar average widths to FGCM1 ranging from 0.07 m to 0.1 m. The minimum width deposit downstream of LWD2 occurred during Experiment LF in the minimal sand flow with a width of 0.11 m. The maximum width deposit was 0.136 m which occurred during Experiment HF post sand addition. However, Experiment MF had larger average widths than Experiment HF.

Similar to width, the height of the deposits varied for each experiment. Experiment LF created the shortest FGCM1 deposit. Its average height was 0.56 cm for pre sand conditions and 0.88 cm for post sand conditions (Figure 3.12). Experiment MF created a deposit of height 0.75 cm in the minimal sand flow with the deposit increasing to a height of 1.31 cm after sand was added to the system (Figure 3.13). Experiment HF had the tallest deposit overall with average heights of 0.94 cm and 1.25 cm and maximum heights of 2.38 cm and 3.19 cm for pre and post sand deposits (Figure 3.14). LWD2 had similar results with the largest deposit being created during high flow discharge conditions and the smallest created during low flow conditions. The average height of the deposit in Experiment HF pre sand was 1.08 cm and then it enlarged to a height of 1.73 cm. Experiment LF had an initial FGCM2 deposit average height of 0.84 cm that increased to 1.52 cm after sand was added.

With the addition of sand, the deposits grew in height for all experiments. For FGCM1, the deposit grew in average height by 0.31 cm – 0.56 cm for the experiments. For Experiment LF and HF, the average height of FGCM1 increased by 0.32 cm and 0.31 cm respectively. The deposit increased in height the most during Experiment MF

where the deposit grew from an average height of 0.75 cm to 1.31 cm with the addition of sand to the system. LWD2 height increases with the addition of sand were 0.68 cm, 0.51 cm, and 0.65 cm for Experiment LF, Experiment MF, and Experiment HF respectively. The erosional and depositional processes that occurred along FGCM1 for each experiment will be reported in the next section.

Table 3.2 Geometry of the FGCM deposit downstream of LWD 1

Experiment	Length (m)	Average Width (m)	Max Width (m)	Average Height (cm)	Max Height (cm)
LF pre sand	3.3	0.081	0.155	0.56	1.85
LF post sand	3.5	0.096	0.152	0.88	2.23
MF pre sand	3.3	0.072	0.12	0.75	1.85
MF post sand	3.45	0.086	0.131	1.31	2.57
HF pre sand	3.4	0.088	0.142	0.94	2.38
HF post sand	3.3	0.107	0.17	1.25	3.19

Table 3.3 Geometry of the FGCM deposit downstream of LWD 2

Experiment	Length (m)	Average Width (m)	Max Width (m)	Average Height (cm)	Max Height (cm)
LF pre sand	1.12	0.0823	0.11	0.84	2.21
LF post sand	0.85	0.0939	0.126	1.52	3.61
MF pre sand	1.2	0.0918	0.124	1.31	2.46
MF post sand	1.1	0.1034	0.13	1.82	4.57
HF pre sand	1.05	0.0795	0.119	1.08	2.91
HF post sand	1.15	0.0897	0.136	1.73	3.14

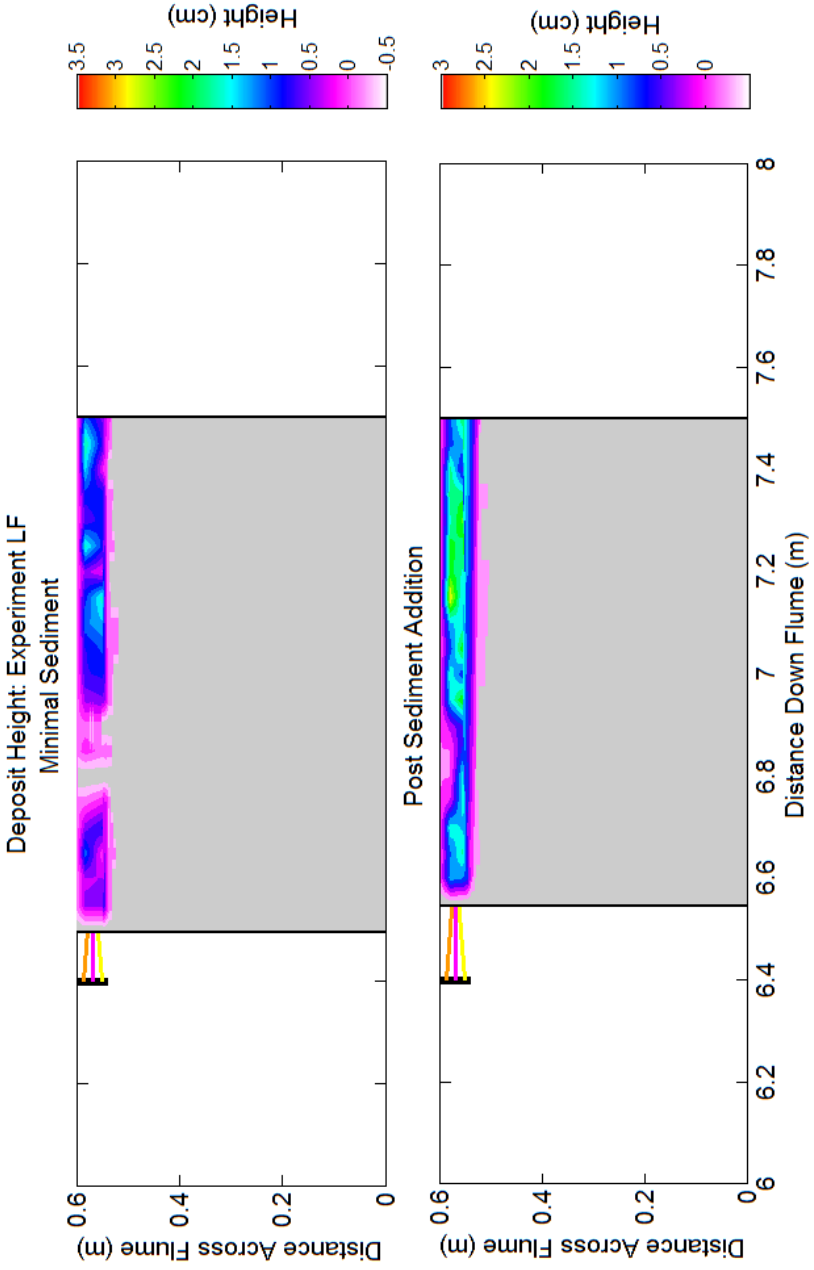

Figure 3.12 Deposit Topography downstream of LWD1 for Experiment LF pre and post sediment addition. Gray color represent areas with little or no sand deposition. These gray areas were not considered a part of the FGCM deposit. Magenta colors are areas where the deposit was seen but could not be measured with a point gauge. Other colors represent the height of the deposit in centimeters.

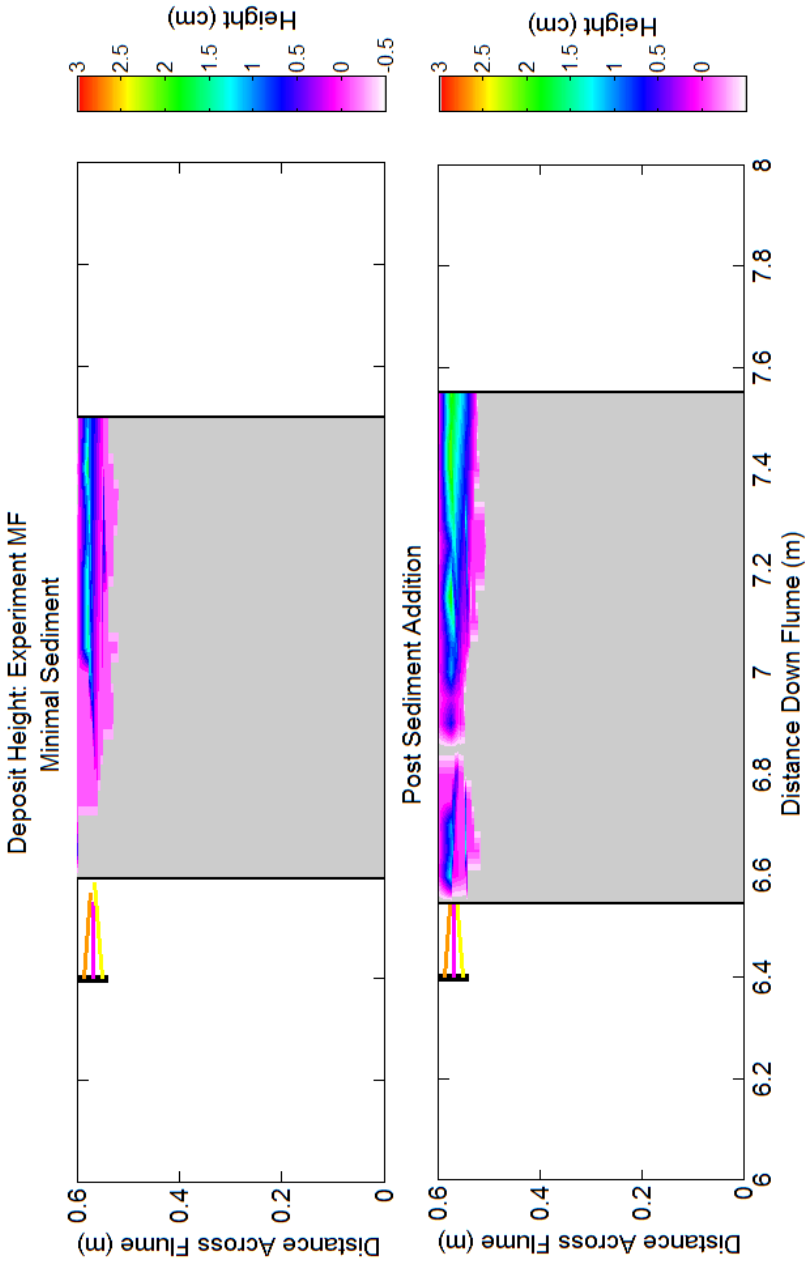

Figure 3.13 Deposit Topography downstream of LWD1 for Experiment MF pre and post sediment addition. Gray color represent areas with little or no sand deposition. These gray areas were not considered a part of the FGCM deposit. Magenta colors are areas where the deposit was seen but could not be measured with a point gauge. Other colors represent the height of the deposit in centimeters.

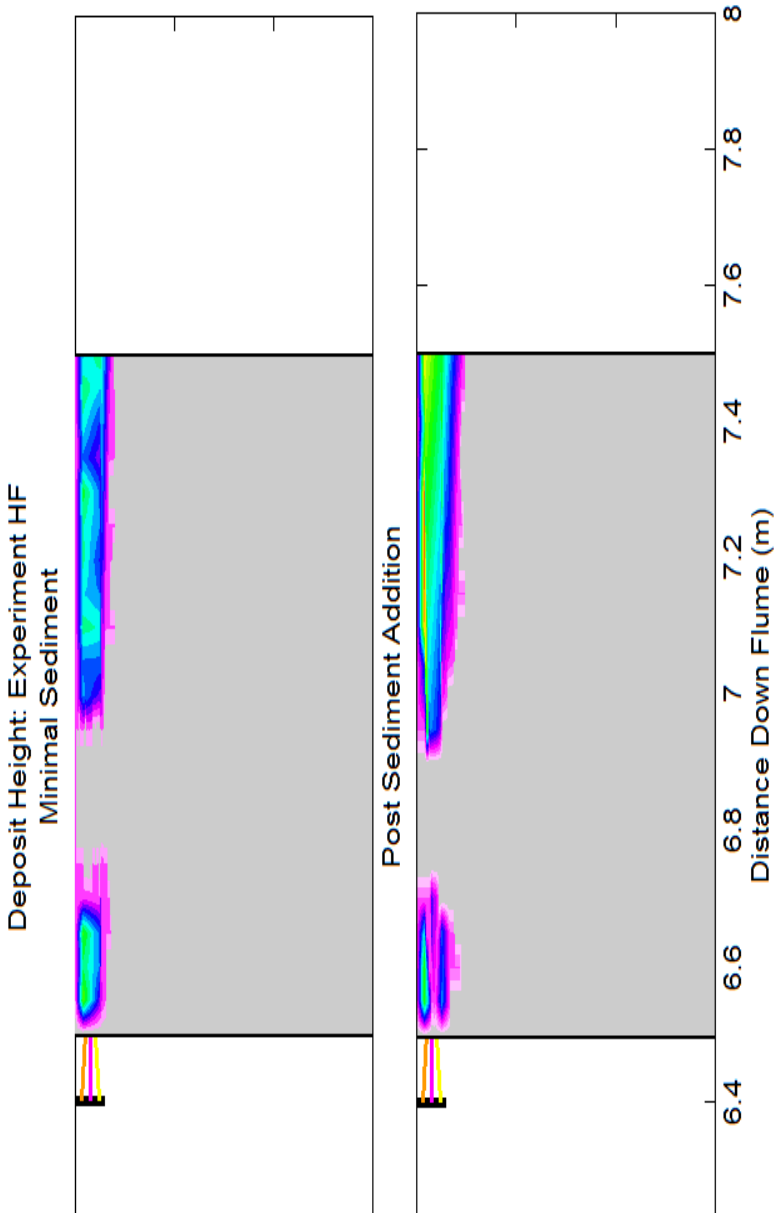

Figure 3.14 Deposit Topography downstream of LWD1 for Experiment HF pre and post sediment addition. Gray color represent areas with little or no sand deposition. These gray areas were not considered a part of the FGCM deposit. Magenta colors are areas where the deposit was seen but could not be measured with a point gauge. Other colors represent the height of the deposit in centimeters.

3.9 Deposit Erosion and Deposition

Deposit height, as discussed in the previous section, was recorded for both minimal and added sediment stages in two downstream transects. Continuous deposit heights were interpolated in MATLAB. The interpolated grid of deposit heights allowed for a difference to be calculated between minimal and added sediment deposits. The difference between each deposit shows where erosion and deposition occurred.

Two diagrams of deposition and erosion were created for each experiment: a process identification map and a change quantification map (Figures 3.15, 3.16, 3.17). The process identification figure (top map) classifies where erosion (red) and deposition (blue) occurred along the deposit. No change (white) was not mapped due to contouring errors. The change quantification map (bottom map) shows how much erosion and deposition occurred. Some of the erosion and deposition identified in the top map is displayed as no change in the bottom map. These areas were areas that altered from minimal sand cover that was not measurable to no sand cover or vice versa. The change thus was not quantifiable.

In Experiment LF, deposition occurred mainly along the ridge of the deposit (Figure 3.9). The cut zone (Figure 3.8) in the minimal sediment stage was filled in. Minimal erosion occurred at 7.1 m downstream. Some erosion was also seen along the wall at 0.6 m in the cross stream direction. Net change between the first and second deposits were 2.74 cm^3 with net erosion being -0.25 cm^3 and net deposition being 2.99 cm^3 (Table 3.4).

In Experiment MF, deposition also occurred along the ridge of the deposit. Deposition also occurred immediately downstream of the LWD. Most of this deposition was not quantifiable though because the deposit went from no sand to

mostly minimal sand cover downstream of the LWD obstruction. Erosion occurred along the deposit near the channel center. Erosional processes created a cut zone and moved some sand away from the ridge sides. The net erosion for Experiment MF was -0.16 cm^3 and net deposition was 1.77 cm^3. Overall, the deposit had a positive change of 1.62 cm^3 with the addition of sand.

Experiment HF differed from the previous two experiments in that there was significant erosion downstream of the LWD obstruction and little erosion near the wall. Net erosion for this experiment was -0.68 cm^3. Deposition of sand occurred after the cut zone, similar to Experiment MF. Deposition, however, was not limited to the ridge and occurred across the deposit. Net deposition was 2.34 cm^3. The net change in deposit size with the addition of sand was 1.65 cm^3.

Table 3.4 Net deposition, erosion, and change for each experiment.

Experiment	**Deposition (cm^3)**	**Erosion (cm^3)**	**Change (cm^3)**
Experiment LF	2.99	-0.25	2.74
Experiment MF	1.87	-0.20	1.67
Experiment HF	2.34	-0.68	1.65

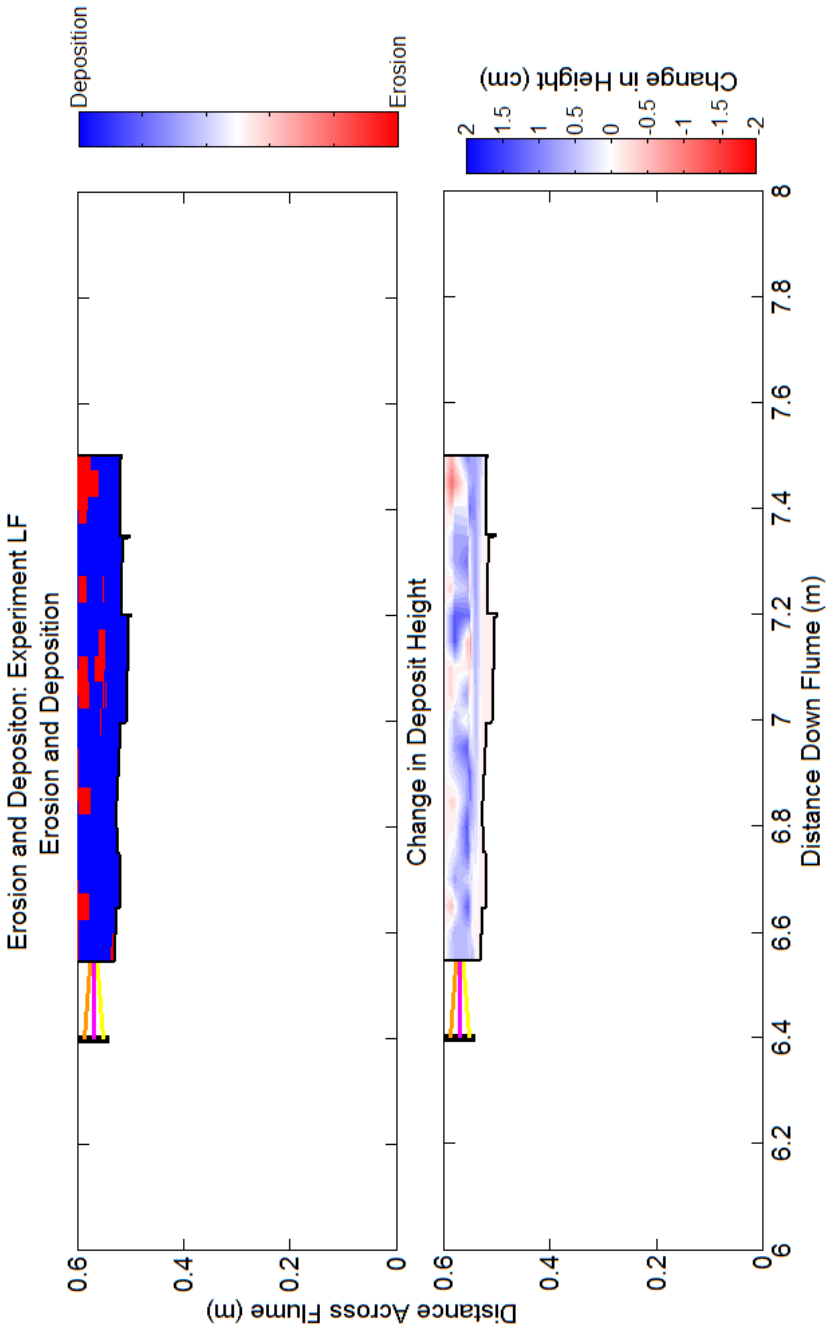

Figure 3.15 Erosion and Deposition processes that occurred downstream of LWD1 between pre and post sediment addition for Experiment LF. The top map shows solely where erosion and deposition occurred. The bottom map quantifies the movement of sediment between pre and post sediment addition.

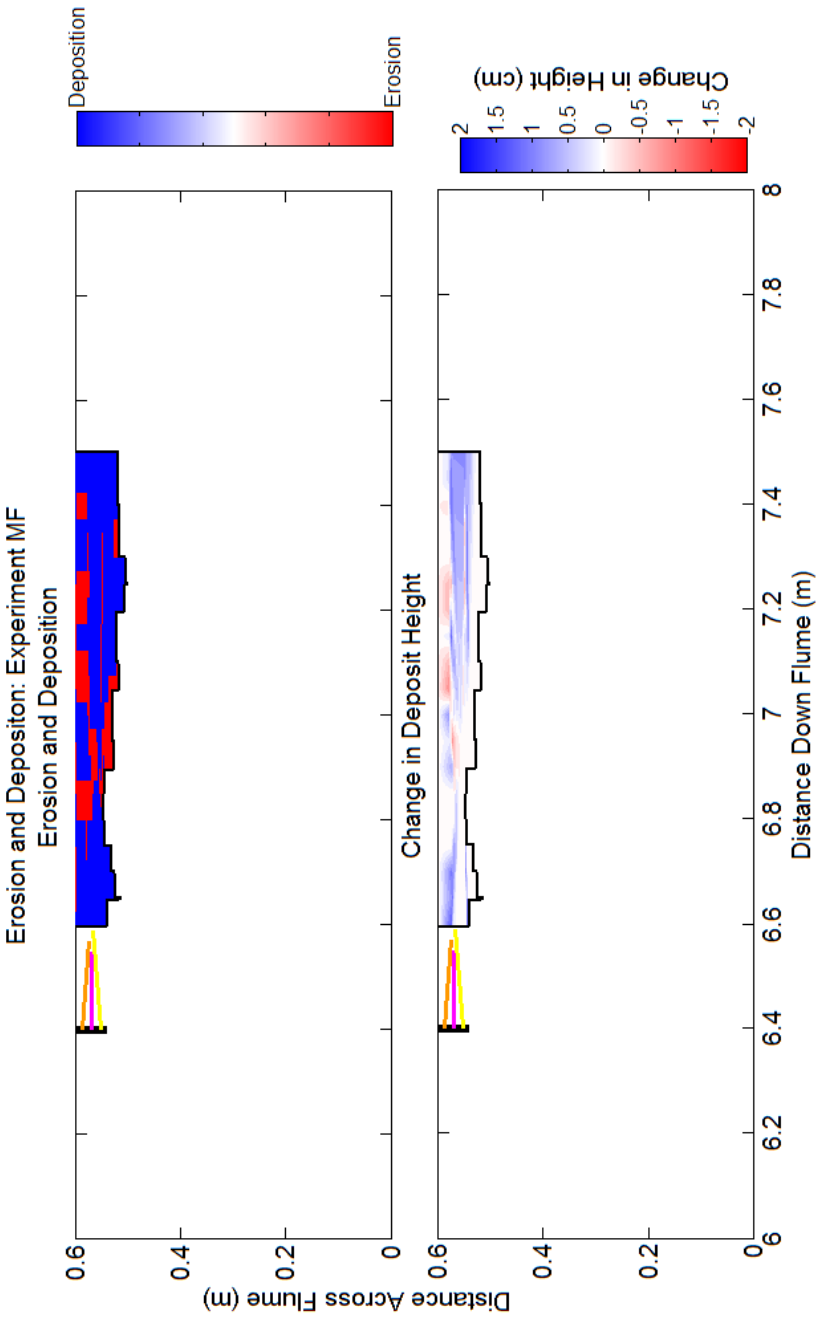

Figure 3.16 Erosion and Deposition processes that occurred downstream of LWD1 between pre and post sediment addition for Experiment MF. The top map shows solely where erosion and deposition occurred. The bottom map quantifies the movement of sediment between pre and post sediment addition.

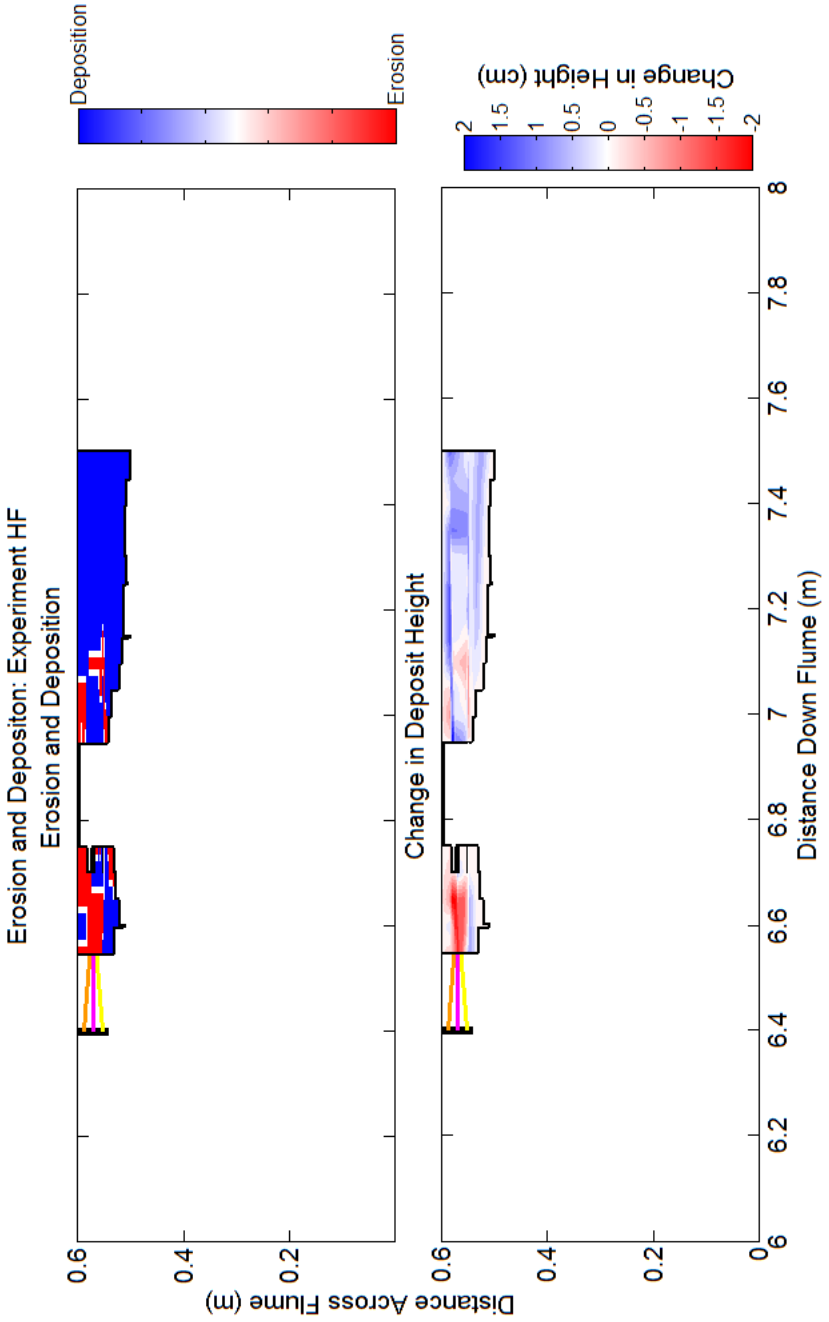

Figure 3.17 Erosion and Deposition processes that occurred downstream of LWD1 between pre and post sediment addition for Experiment HF. The top map shows solely where erosion and deposition occurred. The bottom map quantifies the movement of sediment between pre and post sediment addition.

3.10 Model Scaling

3.10.1 Geometric Scaling

Length values were compared from model results to prototype conditions to check geometric scaling parameters (Table 3.5, 3.6, 3.7). The channel width and length was $2.7 \cdot 10^{-2}$ and $7.6 \cdot 10^{-2}$ times smaller than the prototype conditions. Generally, the model channel and deposit conditions were two orders of magnitude smaller than the prototype. The exceptions to this scale ratio were sediment sizes and deposit length; these variables were only one order of magnitude smaller than prototype conditions.

Ratios of certain length variables of channel and deposit features (Table 3.8) were also calculated for the South River prototype, South River average, and model conditions to compare results of the experiments to the field system. The channel depth to channel width ratio was three times greater in the model than in the prototype. The deposit width to LWD width ratio for the models best matched the ratio of the South River average conditions. No trend was seen among the deposit thickness to water depth ratios nor the deposit width to deposit length ratios.

Table 3.5 Model to prototype length scale ratios for Experiment LF

Property	South River Prototype Conditions (m)	South River Average Conditions (m)	Experiment LF Conditions (m)	Model to Prototype Scale
Channel width	22.5	30	0.60	$2.7 \cdot 10^{-2}$
Channel depth	1	1	$7.6 \cdot 10^{-2}$	$7.6 \cdot 10^{-2}$
LWD length across channel	11	5.6	0.125	$1.1 \cdot 10^{-2}$
Deposit width	5	5	$9.6 \cdot 10^{-2}$	$1.9 \cdot 10^{-2}$

Deposit length	10	25	3.5	0.35
Deposit thickness	0.34	0.34	$9 \cdot 10^{-3}$	$2.6 \cdot 10^{-2}$
Bed sediment	$2.55 \cdot 10^{-2}$	2.55•10-2	$4.5 \cdot 10^{-3}$	0.18
Suspended sediment	$1.25 \cdot 10^{-5}$	1.25•10-5	$1.0 \cdot 10^{-5}$	0.8

Table 3.6 Model to prototype length scale ratios for Experiment MF

Property	**South River Prototype Conditions (m)**	**South River Average Conditions (m)**	**Experiment MF Conditions (m)**	**Model to Prototype Scale**
Channel width	22.5	30	0.60	$2.7 \cdot 10^{-2}$
Channel depth	1	1	$8.5 \cdot 10^{-2}$	$8.5 \cdot 10^{-2}$
LWD length across channel	11	5.6	0.125	$1.1 \cdot 10^{-2}$
Deposit width	5	5	$8.6 \cdot 10^{-2}$	$1.7 \cdot 10^{-2}$
Deposit length	10	25	3.45	0.35
Deposit thickness	0.34	0.34	$1.3 \cdot 10^{-2}$	$3.9 \cdot 10^{-2}$
Bed sediment	$2.55 \cdot 10^{-2}$	2.55•10-2	$4.5 \cdot 10^{-3}$	0.18
Suspended sediment	$1.25 \cdot 10^{-5}$	1.25•10-5	$1.0 \cdot 10^{-5}$	0.8

Table 3.7 Model to prototype length scale ratios for Experiment LF

Property	**South River Prototype Conditions (m)**	**South River Average Conditions (m)**	**Experiment HF Conditions (m)**	**Model to Prototype Scale**
Channel width	22.5	30	0.60	$2.7 \cdot 10^{-2}$
Channel depth	1	1	$8.7 \cdot 10^{-2}$	$8.7 \cdot 10^{-2}$
LWD length across channel	11	5.6	0.125	$1.1 \cdot 10^{-2}$
Deposit width	5	5	0.11	$2.1 \cdot 10^{-2}$
Deposit length	10	25	3.3	0.33
Deposit thickness	0.34	0.34	$1.3 \cdot 10^{-2}$	$3.7 \cdot 10^{-2}$
Bed Sediment	$2.55 \cdot 10^{-2}$	$2.55 \cdot 10^{-2}$	$4.5 \cdot 10^{-3}$	0.18
Suspended Sediment	$1.25 \cdot 10^{-5}$	$1.25 \cdot 10^{-5}$	$1.0 \cdot 10^{-5}$	0.8

Table 3.8 Geometry ratios of channel and deposit parameters for South River prototype, South River average conditions, and Experiment LF, MF, and HF

Ratio	South River Prototype	South River Average Conditions	Experiment LF	Experiment MF	Experiment HF
Channel depth **:** Channel width	$4.4 \cdot 10^{-2}$	$3.3 \cdot 10^{-2}$	0.12	0.14	0.15
Deposit width **:** Deposit thickness	15	15	11	6.6	8.6
Deposit width **:** LWD width	0.45	0.90	0.77	0.69	0.86
Deposit thickness **:** water height	0.34	0.34	0.12	0.15	0.15

3.10.2 Force Scaling: Dimensionless Numbers

Dimensionless numbers were calculated from the hydraulic conditions of each experiment. The dimensionless numbers were used to compare the results of the physical model to real world conditions. Similar dimensionless numbers established that the conditions present in the physical model were similar to conditions in the field system.

The Froude, flow Reynolds, particle Reynolds, Rouse, and Shields parameters were calculated for each experiment (Table 3.6). The Froude number for the experiments and for South River agreed and were both less than one, the expected condition for gravel-bed rivers. The flow Reynolds numbers were each greater than 500 indicating turbulent flow for the prototype and each experiment. The calculated Rouse numbers for prototype and experiments indicated that the fine sediment would be transported as wash load and the bed material would be transported as bed load. The Shields number for the bed sediment indicated transport of bed material while the

Shields number for the fine sediment specified definite transport of fine material. The relative roughness value indicated that flow was rough.

Table 3.9 Dimensionless number parameters for the South River and the equivalent conditions for the physical model based on the hydraulic conditions of each experiment.

Dimensionless Number	**South River Conditions (Depth=1m)**	**Expected Model Conditions**	**Experiment LF**	**Experiment MF**	**Experiment HF**
Froude	0.38	< 1	0.38	0.42	0.43
Flow Reynolds	$1.2 \cdot 10^{6}$	> 500	$2.5 \cdot 10^{4}$	$3.3 \cdot 10^{4}$	$3.5 \cdot 10^{4}$
Particle Reynolds: Bed	$2.8 \cdot 10^{3}$	> 15	$3.2 \cdot 10^{2}$	$3.4 \cdot 10^{2}$	$3.4 \cdot 10^{2}$
Rouse: Sand	0.8	< 0.8	0.45	0.43	0.42
Rouse: Bed	11	> 2.5	8,41	7.93	7.84
Shields: Sand	8.5	> 0.1	3.3	3.8	3.8
Shields: Bed	$3 \cdot 10^{-2}$	0.01 – 0.1	$7.4 \cdot 10^{-2}$	$8.5 \cdot 10^{-2}$	$8.5 \cdot 10^{-2}$
Relative Roughness	39	-	16	19	19

Chapter 4

DISCUSSION

4.1 Physical Scaling

The experimental physical model satisfied a distorted FSM scaling approach to simulate South River, VA conditions at a smaller geometric scale. The vertical to horizontal ratio was distorted as evidenced by the channel depth to channel width ratio being three times greater for the model than the prototype. Sediment sizes were not scaled geometrically; however, the dimensionless numbers satisfy criteria for appropriate sediment transport. The Rouse number correctly bed load transport of the bed material and suspended transport of the fine material in the model flume. The Froude number is also consistent for the South River and model conditions. The dimensionless parameters meet most of the expected conditions and were of similar magnitude for model and prototype. The parameters classified the flow as being turbulent and rough with correct sediment transport of the fine material and the bed sediment. Based on the dimensionless parameters primarily agreeing, the model results can be used to interpret the prototype processes.

4.2 Hydraulic Conditions

The presence of LWD along channel margins influences fluid flow throughout the channel. The LWD obstructs and slows flow, creating a large area of backwater upstream in which water pools. In front of the LWD obstruction, fluid flow slows along the channel margin is pushed flow into the center of the channel (Figure 4.1). The increase of water in the channel center causes water velocity accelerate toward the channel center. After the wood, a portion of the channel flow moves back toward the channel margin behind the LWD in a recirculation current. At the wall of the channel,

there is a reattachment point of flow where a portion of flow rejoins the primary direction of flow downstream while some of the flow moves upstream behind the wood. The upstream flow is evidenced by the upstream migrating ripples in the FGCM deposits a short distance downstream of the LWD. Upstream flow behind the LWD was also detected by velocity measurements in Experiment HF.

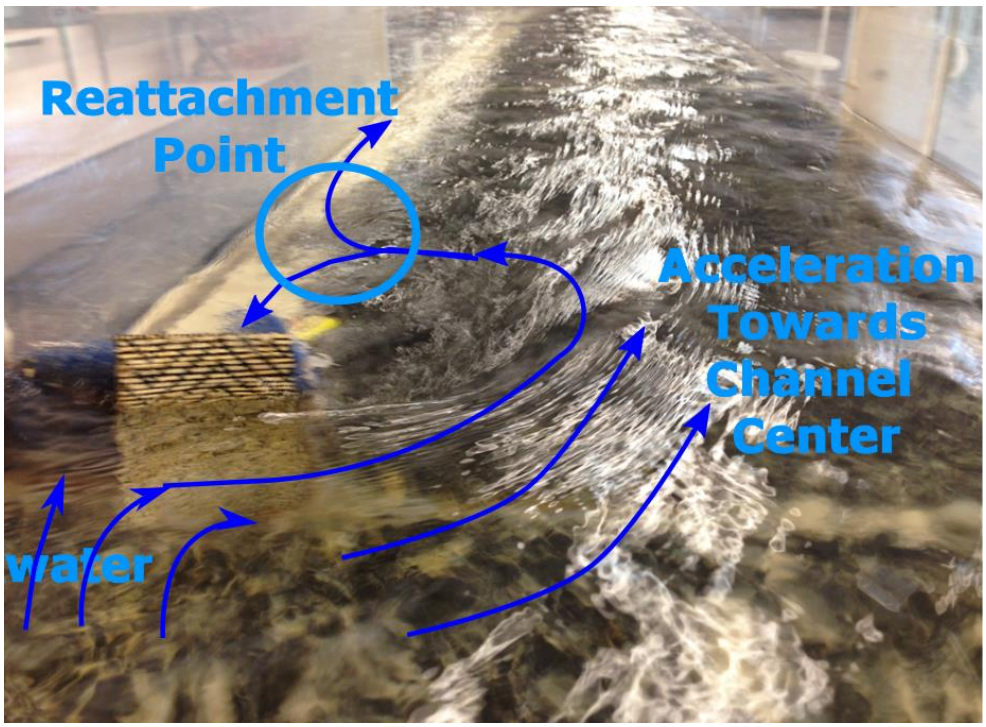

Figure 4.1 Hydraulic conditions influenced by the presence of LWD.

4.3 Shear Stress and Turbulent Kinetic Energy

The boundary shear patterns estimated from the Reynolds Shear and from TKE measurements show similar patterns. The LWD in all experiments created an area of low shear downstream of the wood. These areas of low shear values indicate possible

deposition of sediment. Downstream of the wood at 0.45 m to 0.25 m was an area of high shear stress which would indicate sediment transport in the channel center. The change from high shear to low shear behind the wood would allow fine sediment to settle out of suspension. The LWD also created a high TKE downstream of the wood at 6.7 m, 0.45 m cross-stream. The high TKE values here indicate eddies being shed off the structure. The turbulence would also contribute to sediment transport by keeping particles in suspension.

4.4 Sediment Transport

For rough flows, such as gravel-bed rivers, the critical Shields stress is typically assumed to be within the range of 0.030 to 0.073 (Figure 3.6) (Buffington and Mongtomery 1997). If this threshold is exceeded, sediment transport occurs. If the calculated dimensionless shear stress is below the critical shear, sediment deposition occurs.

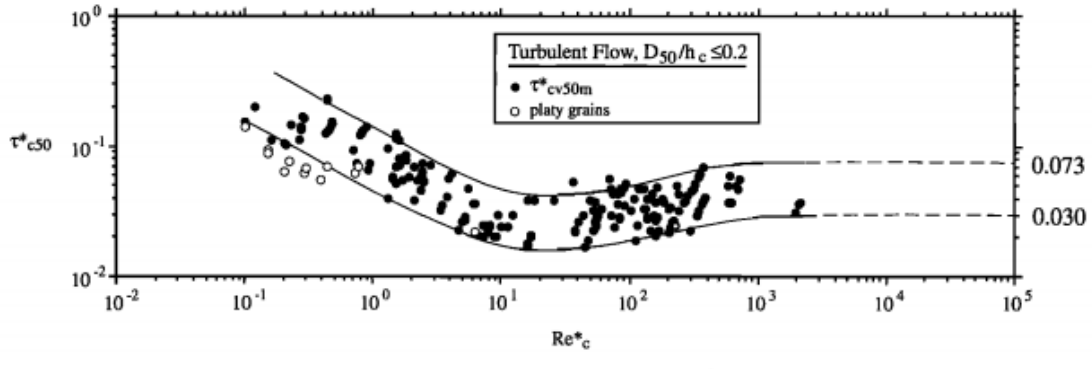

Figure 4.2 Shields entrainment diagram identifying the critical shear stress as a range of values from 0.030 to 0.073 (Buffington and Montgomery 1997).

In all experiments, flow was deemed rough by the particle Reynolds number and the relative roughness constant. Rough flow indicates that the dimensionless shear stress can be compared to a critical Shields value between 0.03 and 0.073.

In all experiments, an area of decreased shear stress is seen downstream of the LWD along the channel margin. In this area of reduced shear stress, the $\tau_*$for Experiment LF are all below 0.03 from 6.7 m to 9 m downstream along the channel margin. The dimensionless shear values are thus less than the critical shear indicating deposition of the fine in this area. For Experiment MF, the dimensionless shear is less than a critical shear value of 0.073 at 7 m downstream along the channel margin. At this locations, deposition is seen in the experiment. At 6.7 m downstream, τ_* is 0.20 signifying sediment transport. In Experiment MF, an area of no deposition was near 6.8 m downstream which may be associated to the high shear value at 6.7 m. The high values of shear stress from 8 m to 9 m downstream do not match patterns of erosion and deposition seen along the deposit. For Experiment HF, dimensionless shear values less than 0.03 are located at 6.7 m and 7.5 m downstream while values less than 0.073 were seen at 8 and 8.5 m downstream. At these locations, there was sediment deposition. At 7 m downstream, high dimensionless shear value of 0.26; however, there was deposition at this location. The high shear value may however correlate to the location of the cutzone which spread from 6.75 to 6.95 m downstream due to inconsistencies in repeating sampling locations accurately. The shear values do have some correlation with patterns of sediment transport and deposition.

The shear values for the bed sediment were less than 0.03 throughout the entire channel for all experiments. The low shear values indicate deposition of the bed sediment with minimal transport downstream.

4.5 Deposit Formation

FGCM deposits form as a result of LWD present in the river channel. The LWD creates a zone of low velocity and low shear stress downstream of the obstruction allowing fine sediments to settle out of suspension. Some of the sand is pushed through the blue wire mesh and settles out of suspension. This sand forms the beginning of the deposit and is pushed downstream forming ripples as water and more sediment is transported through the wire mesh (Figure 4.3). The next portion of the deposit is the upstream migrating ripples that are formed by sediment brought into the area of low shear by the recirculating current. Following the upstream migrating ripples is a cutzone area in the two higher discharge experiments. The cutzone is located at the flow reattachment point. Downstream of the reattachment point, flow rejoins the primary flow direction. Here, downstream migrating ripples form as sand is deposited and is pushed downstream by the flow.

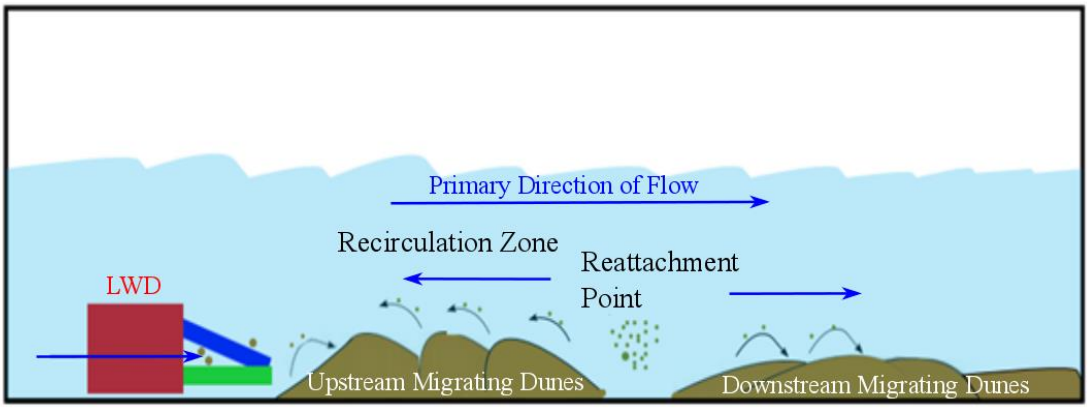

Figure 4.3 Conceptual diagram of sediment transport that forms FGCM deposits downstream of LWD.

The processes that form FGCM deposits downstream of LWD in the experimental flume and in the South River are similar to the processes that form reattachment deposits downstream of debouching debris fans in the Colorado River in Grand Canyon, Arizona (Schmidt 1990). Debris fans that extended into the river obstructed flow creating a zone of recirculating current following flow separation caused by the obstruction. Two types of bars formed due to the new flow pattern: separation bars and reattachment bars (Figure 4.4). The separation bar formed upstream of the reattachment point of flow. Downstream of the primary eddy, reattachment bars formed and were bounded by the primary eddy current, the eddy fence, and the main current. FGCM deposits form in a similar manner as the LWD obstructs flow and constricts flow to the channel center and opposite channel margin. The obstruction creates an area of reduced flow and shear stress in which sediment can accumulate. Sediment is brought into this area by a recirculating current that is formed due to the presence of an obstruction constricting flow.

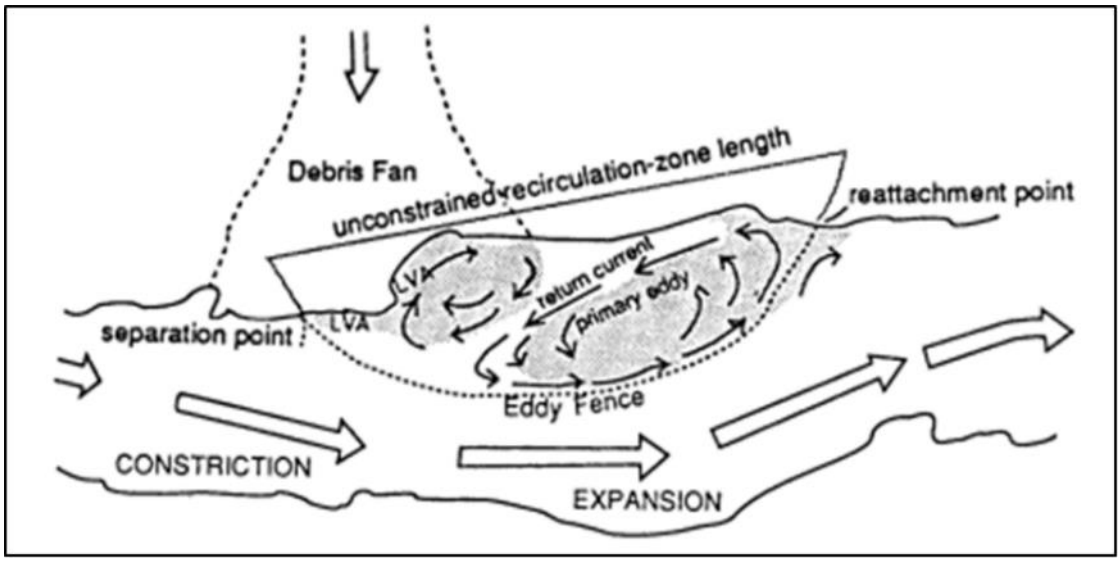

Figure 4.4 Flow patterns created by debouching debris fans at moderate or high discharge. Arrows indicate surface flow direction. The upstream shaded area is the separation bar; the downstream shaded area is the reattachment bar. LVA indicates low velocity area. (Schmidt 1990)

Deposition occurs for all experiments thus a threshold for sediment deposition based on discharge could not be quantified. None of the discharges produced high shear values downstream of the wood that would erode the deposit entirely. However, a much larger quantity of erosion was seen in Experiment HF compared to Experiments LF and MF.

4.6 Deposit Size

The LWD influences flow in the channel which in turn produces conditions prime for sediment deposition. Discharge is also a controlling factor in the deposition of sand. In lower flows, there is seen to be more deposition compared to the high flow experiment. Comparably, the high flow discharge erodes more material than the low flow and medium flow discharge experiments.

The length of the deposit was similar for deposits behind corresponding LWD obstructions for each experiment. The length of the deposit is not influenced by discharge in this study. Rather, the deposit length is controlled by other geomorphic features in the channel. The length of FGCM1 was controlled by the presence of LWD2 on the opposing channel margin. The length of FGCM2 was controlled by the shallowing of channel depth at the end of the flume channel.

The width of the deposits varied across experiments but was similar for both deposits. The width may be controlled by the width of the wood structure and the discharge. At higher flows, the water is pushed more into the center of the channel as evidenced by a zone of high TKE spread across the channel after the wood. The water being pushed away from the wood structure may create a larger zone of low velocity downstream of the wood for sediment deposition. The width of the wood would influence how much of the channel flow is blocked before the zone of low velocity and shear. The ratio of deposit width to wood ranges from 0.76 to 0.90 for all experiments. The deposit width is greatest for Experiment HF which suggest the faster flow is diverted further from the channel margin. The model results ratios are similar to the South River average conditions supporting that the length of the wood into the channel may control the deposit width.

The deposit height may also be influenced by discharge. The tallest deposit was constructed in the medium flow discharge experiment, post sediment addition for both deposits in the channel. The high flow discharge rate had a smaller deposit post sediment addition because the flow was eroding material. The low flow created the smallest deposits possibly because the flow was too small to move material from upstream.

4.7 Application of Study

Knowledge of FGCM deposit formation contributes to the comprehension of fine sediment transport. Fine sediment often is a factor in transporting nutrients and pollutants downstream. The formation of deposits downstream of LWD obstructions indicate a geomorphic setting for contaminants and nutrients. The deposits form under all three discharges explored. Erosion of the deposit was greatest in the high flow condition. Erosion of sediment to be washed out of storage would be expected in flood events while deposition and storage occur mainly in low flow events.

Chapter 5

CONCLUSIONS

5.1 FGCM Formation

FGCM deposits form as reattachment bars downstream of LWD obstructions in the channel margins of gravel-bed rivers. The LWD allows some sediment to pass through the rootwad while creating a recirculating current that delivers additional sediment behind the wood. FGCM deposits formed under the three discharge rates (0.0017, 0.0025, and 0.031 m3/s) studied. The length of the deposits was controlled by geomorphic features within the channel while the width was controlled by the width of the LWD obstruction and discharge. The deposit height may be influenced by discharge rate. The presence of a cut zone is only present in medium to high discharges. Significant erosion of the deposit occurred in the high discharge scenario. Similar results would be expected to occur in field conditions such as the model prototype, South River, VA.

5.2 Study Methods and Future Studies

This study was an exercise to determine the influence of LWD and discharge on the formation of FGCM deposits. The experiments used a distorted FSM scaling approach to assume model results would be expected in prototype conditions. The study simplifies actual river conditions to produce a basic understanding of FGCM formation.

This study can be continued by exploring other discharge rates and sediment concentrations to better quantify how and when these deposits form and erode. Multiple stages of sediment addition could also be investigated to determine if flow or sediment concentration is the yielding factor for maximum deposit size.

REFERENCES

Abbe, T. B., & Montgomery, D. R. (1996). Large woody debris jams, channel hydraulics and habitat formation in large rivers. Regulated Rivers Research & Management, 12(23), 201-221.

Bruton, M. N. (1985). The effects of suspensoids on fish. Hydrobiologia, 125(1), 221-241.

Buffington, J. M., & Montgomery, D. R. (1997). A systematic analysis of eight decades of incipient motion studies, with special reference to gravel-bedded rivers. Water Resources Research, 33(8), 1993-2029.

Daniels, M. D. (2006). Distribution and dynamics of large woody debris and organic matter in a low-energy meandering stream. Geomorphology, 77(3), 286-298.

Daniels, M. D., & Rhoads, B. L. (2003). Influence of a large woody debris obstruction on three-dimensional flow structure in a meander bend. Geomorphology, 51(1), 159-173.

Fetherston, K. L., Naiman, R. J., & Bilby, R. E. (1995). Large woody debris, physical process, and riparian forest development in montane river networks of the Pacific Northwest. Geomorphology, 13(1), 133-144.

Eggleston, J. R. (2009). Mercury Loads in the South River and Simulation of Mercury Total Maximum Daily Loads (TMDLs) for the South River, South Fork Shenandoah River, and Shenandoah River: Shenandoah Valley, Virginia. Reston, VA: US Geological Survey.

Foster, I. D. L., & Charlesworth, S. M. (1996). Heavy metals in the hydrological cycle: trends and explanation. Hydrological processes, 10(2), 227-261.

Gurnell, A., Tockner, K., Edwards, P., & Petts, G. (2005). Effects of deposited wood on biocomplexity of river corridors. Frontiers in Ecology and the Environment, 3(7), 377-382.

Gurnell, A. M., & Gregory, K. J. (1995). Interactions between semi-natural vegetation and hydrogeomorphological processes. Geomorphology, 13(1), 49-69.

Hess, J. M. (2007). Distribution and residence times of large woody debris along South River, Shenandoah Valley, Virginia. ProQuest..

Knighton, D. (1998). Fluvial forms and processes: London. Edward Arnold.

Kondolf, G. M., Sale, M. J., & Wolman, M. G. (1993). Modification of fluvial gravel size by spawning salmonids. Water Resources Research, 29(7), 2265-2274.

Lawler, Matusky & Skelly, Engineers. 1982. Engineering Feasibility Study of Rehabilitating the South River and South Fork Shenandoah River.

Lisle, T. E. (1989). Sediment transport and resulting deposition in spawning gravels, north coastal California. Water resources research, 25(6), 1303-1319.

Mangelsdorf, J., Scheurmann, I. K., & Weiß, D. I. F. H. (1990). Channel Geometry. In River Morphology (pp. 92-140). Springer Berlin Heidelberg.

Miller, J. R. (1997). The role of fluvial geomorphic processes in the dispersal of heavy metals from mine sites. Journal of Geochemical Exploration, 58(2), 101-118.

Nanson, G. C. (1981). New evidence of scroll-bar formation on the Beatton River. Sedimentology, 28(6), 889-891.

Narinesingh, P. (2009). A sinuous gravel-bedded river with frequent bedrock exposures: The statistics of its planform compared with a freely meandering river and the suitability of a processed-based hydraulic model predicting its erosion. University of Delaware.

Owens, P. N., Walling, D. E., & Leeks, G. J. (1999). Deposition and storage of fine-grained sediment within the main channel system of the River Tweed, Scotland. Earth Surface Processes and Landforms, 24(12), 1061-1076.

Schmidt, J. C. (1990). Recirculating flow and sedimentation in the Colorado River in Grand Canyon, Arizona. The Journal of Geology, 709-724.

Smith, R. D., Sidle, R. C., & Porter, P. E. (1993). Effects on bedload transport of experimental removal of woody debris from a forest gravel-bed stream. Earth Surface Processes and Landforms, 18(5), 455-468.

Petts, G. (1984). Impounded Rivers. Wiley: Chichester.

Ralph, S. C., Poole, G. C., Conquest, L. L., & Naiman, R. J. (1994). Stream channel morphology and woody debris in logged and unlogged basins of western Washington. Canadian Journal of Fisheries and Aquatic Sciences, 51(1), 37-51.

Peakall, J., Ashworth, P., & Best, J. (1996). Physical modelling in fluvial geomorphology: principles, applications and unresolved issues. The scientific nature of geomorphology, 221-253.

Phillips, J. M., & Walling, D. E. (1999). The particle size characteristics of fine-grained channel deposits in the River Exe Basin, Devon, UK. Hydrological Processes, 13(1), 1-19.

Pizzuto, J. (2012). Predicting the accumulation of mercury-contaminated sediment on riverbanks—An analytical approach. Water Resources Research, 48(7).

Pizzuto, J. and O'Neal, M. (2009). Increased mid-20th century river bank erosion rates related to the demise of mill dams, South River, Virginia. Geology, 37, 19.

Pizzuto, J.E., Skalak, K.J., O'Neal, M., Narinesingh, P., Rhoades, R., and Hess, J. (2006). Geomorphology of the South River between Waynesboro and Port Republic, VA: Geomorphic characterization and sediment budget for silt and clay. Unpub. Technical Report, 14 chapters.

Pomraning, S. (2011). Determing the Residence Time of Mercury-Contaminated Fine-Grained Sediment in the Hyporheic Zone of a Gravel Bed River Using Radionuclid Dating Methods. M.S. Thesis, Univeristy of Delaware, Newark, DE.

Rhoades, E. L., O'Neal, M. A., & Pizzuto, J. E. (2009). Quantifying bank erosion on the South River from 1937 to 2005, and its importance in assessing Hg contamination. Applied Geography, 29(1), 125-134.

Ritter, D. F., Kochel, R. C., & Miller, J. R. (2011). Process Geomorphology. Long Grove, IL: Waveland Press.

Schmidt, J., Parnell, R., Grams, P., Hazel, J., Kaplinski, M., Stevens, L., & Hoffnagle, T. (2001). The 1996 controlled flood in Grand Canyon: hydrology, hydraulics, sediment transport, and geomorphic change. Ecological Applications, 11: 657-671.

Skalak, K. J. (2009). Fine-grained channel margin deposits in a typical gravel bed river: Spatial and temporal controls on the distribution, quantity, and residence time and implications for centennial-scale sediment and mercury cycling. University of Delaware.

Skalak, K., & Pizzuto, J. (2010). The distribution and residence time of suspended sediment stored within the channel margins of a gravel-bed bedrock river. Earth Surface Processes and Landforms, 35(4), 435-446.

Webb, A. A., & Erskine, W. D. (2003). Distribution, recruitment, and geomorphic significance of large woody debris in an alluvial forest stream: Tonghi Creek, southeastern Australia. Geomorphology, 51(1), 109-126.

Wilcock, P. R., Kenworthy, S. T., & Crowe, J. C. (2001). Experimental study of the transport of mixed sand and gravel. Water Resources Research, 37(12), 3349-3358.

Wolman, M. G. (1954). A method of sampling coarse river-bed material. EOS, Transactions American Geophysical Union, 35(6), 951-956.

Wood, P. J., & Armitage, P. D. (1997). Biological effects of fine sediment in the lotic environment. Environmental management, 21(2), 203-217.